Journal of Materials Science: Materials in Medicine (2025)36:23
https://doi.org/10.1007/s10856-025-06872-9

BIOCOMPATIBILITY STUDIES

Original Research

Enhanced osteogenic capacity of octacalcium phosphate involving adsorption of stromal-derived factor-1 in a standardized defect of a rat femur

Ryuichi Kanabuchi[1,2] · Ryo Hamai[1] · Yu Mori[2] · Soshi Hamada[2] · Yukari Shiwaku[1] · Yuko Sai[1] · Kaori Tsuchiya[1] · Toshimi Aizawa[2] · Osamu Suzuki[1]

Received: 11 November 2024 / Accepted: 17 February 2025

Abstract

This study investigated whether octacalcium phosphate (OCP) enhances bone regeneration through its synergistic effect with stromal-derived factor-1 (SDF-1). Recombinant SDF-1 (0.5–5.0 μg) was combined with OCP granules through lyophilization. OCP/SDF-1 granules were implanted into a rat femoral standardized defect for 2 and 4 weeks and subjected to histomorphometry, C-X-C motif chemokine receptor 4 (CXCR4) and osteocalcin immunohistomorphometry, and tartrate-resistant acid phosphatase (TRAP) staining. Calcium-deficient hydroxyapatite (CDHA) was used as a control for in vitro analyses. Mesenchymal stem cell (MSC) migration was estimated using a Transwell system with OCP/SDF-1. SDF-1 release from OCP/SDF-1 into the supernatant was determined without cells. SDF-1 adsorption in 4-(2-hydroxyethyl)-1-piperazineethanesulfonic acid buffer onto OCP, the chemical structure of OCP immersed in the medium using Fourier transform infrared spectroscopy, and the degree of supersaturation of the medium were determined. Bone regeneration and OCP degradation were enhanced the most by 1.0 μg of OCP/SDF-1 at 2 weeks after implantation by CT analysis and increasing CXCR4-positive, osteocalcin-positive, and TRAP-positive cells accumulation around the OCP. MSC migration increased until 48 h in the following order: SDF-1 only, CDHA/SDF-1, and OCP/SDF-1, with the greatest effect with 1.0 μg of SDF-1 than from OCP. CDHA promoted a greater release than OCP at 48 h. The physicochemical analyses indicated that SDF-1 interacted with OCP through Freundlich-type adsorption and that the adsorption controlled SDF-1 release from OCP during the hydrolysis into CDHA. Therefore, leveraging its molecular affinity for the OCP surface, OCP/SDF-1 facilitates MSC migration and enhances bone formation by ensuring the controlled, sustained release of SDF-1 from OCP.

Graphical Abstract

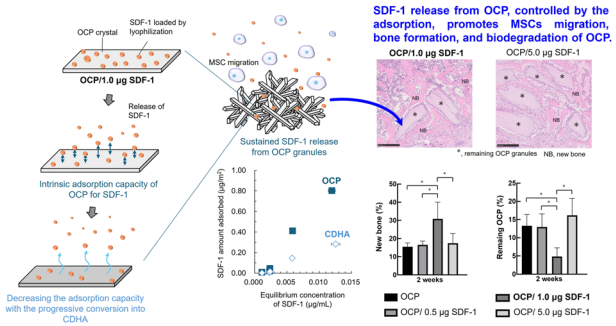

✉ Osamu Suzuki
suzuki-o@tohoku.ac.jp

[1] Division of Craniofacial Function Engineering (Division of Biomaterials Science and Engineering), Tohoku University Graduate School of Dentistry, Sendai, Japan

[2] Department of Orthopaedic Surgery, Tohoku University Graduate School of Medicine, Sendai, Japan

Published online: 28 February 2025

1 Introduction

Octacalcium phosphate (OCP, $Ca_8H_2(PO_4)_6 \cdot 5H_2O$) has recently become recognized as a bone substitute material that exhibits highly osteoconductive properties than existing calcium phosphate materials, such as hydroxyapatite (HA, $Ca_{10}(PO_4)_6(OH)_2$) [1–5]. OCP is a precursor for the formation of HA in aqueous solution [6, 7] and is considered a precursor of bone apatite crystals [8]. OCP has been identified as a precursor of bone apatite crystals with non-collagenous protein osteocalcin in humans and rats [9], the protein affinity of which was similar to the osteocalcin accumulation behavior when OCP is implanted into a bone defect [10] and also to a high affinity for tissue-specific proteins and serum proteins [1, 11–18]. Further studies disclosed that OCP exhibited a capacity including small molecules, such as carboxylates [19–21], and some drugs showing antibacterial properties, such as doxorubicin (DOX) [22] and metronidazole [23], can be incorporated within the structure or adsorbed onto the surface. However, the interaction between OCP and specific molecules involved in bone-tissue-related cells function and its effect on osteogenic activity have not been clarified.

OCP is a metastable phase at physiological pH and undergoes irreversible phase transformation into non-stoichiometric calcium-deficient hydroxyapatite (CDHA) in vitro and in vivo [1, 2, 7, 24–29]. There is a general consensus that the phase transformation of OCP to CDHA is initiated spontaneously [7, 30–32]. OCP hydrolysis results in a slight decrease in pH adjacent to the surface owing to the occurrence of an inorganic ion gradient environment induced by hydrolysis advancement [28, 33]. In vitro analyses of cellular responses to OCP substantiated the following cellular activating properties: (1) osteoblast differentiation of bone marrow stromal cells in a dose-dependent manner [34], (2) osteocyte differentiation from mesenchymal stem cells (MSCs) in vitro and osteoblast precursor cells in vivo in a non-contact manner with OCP [35, 36], (3) formation of osteoclasts in a co-culture of osteoblasts and bone marrow macrophages without the addition of receptor activator of NF-kappaB ligand, an osteoclast differentiation factor [37], which explains the superior biodegradability of OCP material in vivo in comparison with other existing calcium phosphate materials such as HA and β-tricalcium phosphate [10], (4) migration of macrophages, which are osteoclast precursor cells [38], (5) capillary-like tube formation of human umbilical vein endothelial cells [39], (6) accumulation and differentiation of committed osteoblast progenitors (leptin receptor-expressing bone marrow-derived MSCs) around the material [40].

Although OCP is a material with high potential for clinical application based on the bone tissue-related cellular activating capacity explained above [10, 34–40], the bone graft treatment, in particular autografts, is still widely used [41, 42]. This is because autologous bone is recognized as the most reliable bone replacement material that stems from the inclusion of cellular components, growth factors, and cellular scaffold materials (collagen and bone apatite crystals) [43]. In a direct comparison of bone regeneration in rat calvarial bone defect implantation between OCP granules and autologous bone, superior bone regeneration was observed with autologous bone [44]. However, when autologous bone and OCP are combined, osteoblast activation occurs because of the chemical interaction of OCP with autologous bone apatite crystals through crystal dissolution and re-precipitation mechanisms [44]. These results further strengthen the rationale for using OCP for bone regeneration [45]. There may be several manners to increase the bone regeneration of OCP, which can be achieved by modifying the material properties themselves [46, 47], increasing the bone regeneration ability by combining MSCs [48] using conventional tissue engineering techniques, or adding growth factors [5].

C-X-C motif chemokine ligand 12 (CXCL12), also known as stromal-derived factor-1 (SDF-1), is a chemokine belonging to the CXC family [49]. A chemokine is a small secreted protein with four cysteine residues linked by two disulfides in two cysteine residues [50–53]. SDF-1 is considered to play a chemotactic role in MSCs by increasing cell motility gene expression [49] and recruiting endothelial precursor cells to tissue-regenerating portions [54]. It has been reported that SDF-1 can be incorporated into scaffold materials, such as poly (lactide-co-glycolide) [55] and HA materials [56]. The effect of SDF-1 on OCP, the molecular interaction between SDF-1 and OCP, and the sustained release characteristics of OCP when adsorbed on the material are not yet known. However, because OCP has a unique structure consisting of apatite and hydrated layers [6], we expected that OCP might function as a good adsorbent for SDF-1, resulting in the possible enhancement of the synergistic effect on bone formation.

This study investigated whether there is a synergistic effect between OCP and SDF-1. Therefore, we investigated the histomorphometry of bone regeneration after OCP/SDF-1 implantation in femoral bone defects in vivo, migration of MSCs in the presence of OCP in vitro, adsorption capacity of OCP for SDF-1 in vitro, sustained release behavior of SDF-1 from OCP/SDF-1, and hydrolysis characteristics of OCP during release in vitro in comparison with CDHA prepared from OCP hydrolysis [2, 14, 40].

2 Materials and methods

2.1 Preparation of SDF-1-loaded OCP and CDHA granules

Both OCP and CDHA were prepared in the laboratory according to the methods previously reported. OCP was

prepared from a supersaturated solution with respect to OCP and HA using the direct precipitation method [1]. CDHA was synthesized by hydrolyzing the original OCP with constant stirring at 65 °C for 48 h [14]. The synthesized OCP and CDHA were sieved to prepare granules with a particle size of 300–500 μm. The granules were sterilized by dry heating at 120 °C for 2 h, instead of autoclaving sterilization to avoid partial collapse of the crystal structure of OCP [1, 2].

Recombinant human SDF-1α (300-28 A, PeproTech, Inc., Rocky Hill, NJ, USA) was dissolved at 0.02, 0.04, and 0.20 μg in 1 μL of phosphate buffer saline (PBS) and then sterilized using Millipore filters with 0.22-μm pores. Then, 25 μL of PBS containing SDF-1 at 0.02, 0.04, and 0.20 μg/μL was dropped onto 5.0 mg of OCP granules to prepare OCP granules loaded with 0 (OCP), 0.5 (OCP/0.5 μg SDF-1), 1.0 (OCP/1.0 μg SDF-1), and 5.0 μg (OCP/5.0 μg SDF-1) of SDF-1, respectively. The granules were mixed with PBS containing SDF-1 for several seconds. OCP granules with SDF-1/PBS were frozen at −20 °C for 24 h and then lyophilized for 48 h. The CDHA granules loaded with 0 (CDHA) and 1.0 μg (CDHA/1.0 μg SDF-1) of SDF-1 were also prepared using the methods described above.

The morphologies of OCP and CDHA before and after the loading of 1.0 μg SDF-1 were observed using a scanning electron microscope (SEM, JSM-6390LA; JEOL LTD., Tokyo, Japan) at an acceleration voltage of 10 kV. The specimens for SEM observations were coated with Pt.

2.2 In vitro experiments

2.2.1 MSC migration assay

Mouse bone marrow-derived MSC line D1 cells (ATCC, Rockville, Maryland, USA) were maintained in a culture medium in 5% CO_2 and 95% air atmosphere under humidified conditions at 37 °C. The medium consisted of high-glucose Dulbecco's modified Eagle's medium (Fujifilm Wako Pure Chemical Co., Osaka, Japan), 10% fetal bovine serum (Biosera Inc.), and 1% penicillin-streptomycin mixed solution (Nacalai Tesque, Inc., Kyoto, Japan). Then, 5.0 mg of OCP/0.5 μg SDF-1 ($n = 3$), OCP/1.0 μg SDF-1 ($n = 3$), OCP/5.0 μg SDF-1 ($n = 3$), CDHA/1.0 μg SDF-1 ($n = 3$), OCP, and CDHA ($n = 3$) were placed on the bottom of 24-well plates and soaked in 800 μL of culture media. Subsequently, a Transwell (Cell Culture Insert, 8.0 μm pore size, FALCON®; Corning Inc., Corning, NY, USA) was applied to each well. D1 cells (passage 5–6) were seeded on the Transwell at 9.9×10^4 cells/well and incubated in 1.1 mL of culture medium in 5% CO_2 and 95% air atmosphere under humidified conditions at 37 °C for 48 h. D1 cells in the absence of SDF-1 were used as a control group. Cells in the culture medium supplemented with PBS containing SDF-1 (final amount in the medium: 1.0 μg) were incubated as 1.0 μg SDF-1 group.

At 48 h, the incubated cells were collected using trypsin-EDTA (Nacalai Tesque, Inc.) to count the number of cells in the Transwell. The percentage of cells migrating from the surface of the Transwell to the OCP/SDF-1 or CDHA/SDF-1 was calculated using Eq. (1):

$$\text{Cell migration rate}(\%) = \frac{N_0 - N_{48h}}{N_0} \times 100 \quad (1)$$

N_0 and N_{48h} represent the initial and remaining cell numbers at 48 h in the Transwell, respectively.

2.2.2 Change in SDF-1 concentration in media and SDF-1 release rate from OCP or CDHA granule

Five milligrams of OCP/SDF-1 (0.5, 1.0, and 5.0 μg SDF-1) and CDHA/SDF-1 (1.0 μg SDF-1) were incubated in 1.1 mL of culture media in the absence of D1 cells in 5% CO_2 and 95% air atmosphere under humidified conditions at 37 °C for 3, 6, 24, and 48 h. After incubation, culture medium supernatants were collected through centrifugation. The concentrations of SDF-1 in the collected supernatants were determined using human SDF-1α ELISA (900-K92, Peprotech Inc.). The concentrations in the culture media supplemented with 1.0 μg/mL SDF-1 were measured after incubations at 3, 6, 24, and 48 h. The release rates of SDF-1 from OCP and CDHA were estimated using the measured SDF-1 concentrations for each incubation period.

2.2.3 Adsorption test

The adsorption of SDF-1 onto OCP and CDHA was examined in the buffer, simulating the physiological environment. First, 100 mM 4-(2-hydroxyethyl)-1-piperazineethanesulfonic acid (HEPES)- 50 mM NaCl containing 0.5 mM Ca^{2+} and 0.5 mM Pi ion (pH 7.4, 37 °C) was prepared. The buffer was prepared to be saturated and supersaturated with respect to OCP and HA, respectively [57]. SDF-1 (PeproTech) was dissolved in HEPES buffer at concentrations of 0.05, 0.075, 0.10, 0.25, and 0.50 μg/mL. OCP (16 m^2/g) and CDHA (45 m^2/g) granules [14] with a diameter of <53 μm were soaked in the buffer containing SDF-1 with a rotation mixing for 1 h at 5 mg/mL. After incubation, supernatants were collected through centrifugation. The SDF-1 concentration in the supernatants before and after the incubation was determined using a Human CXCL12/SDF-1 alpha ELISA kit (DSA00, R&D Systems, Minneapolis, MN, USA) to estimate the amount of SDF-1 adsorbed onto OCP and CDHA. The adsorption isotherms were approximated using the Freundlich isotherm equation Eq. (2):

$$W = K_f \cdot C^{1/n} \quad (2)$$

Where W is the amount of adsorbate adsorbed, C is the equilibrium adsorbate concentration, and K_f and n are adsorption parameters.

2.2.4 Change in Ca^{2+} and inorganic phosphate (Pi) ion concentration and pH in cell culture media

The supernatants of culture media incubated with OCP, OCP/SDF-1 (0.5, 1.0, and 5.0 μg SDF-1), CDHA, and CDHA/SDF-1 (1.0 μg SDF-1) granules were collected at 48 h. Chemical analysis kits were used to determine the concentrations of Ca^{2+} and Pi ions in the culture medium (Calcium E and Phosphor C tests; Fujifilm, Wako Pure Chemical Co.). The pH of the supernatants was measured using a pH electrode (9616S-10D; HORIBA, Ltd., Kyoto, Japan).

The degree of supersaturation (DS) with respect to OCP, HA, and DCPD in the culture media incubated with SDF-1-loading OCP and CDHA granules was calculated using Eq. (3):

$$DS = \left(\frac{IP}{K_{sp}}\right)^{\frac{1}{\nu}} \quad (3)$$

Where IP, K_{sp}, and ν are ionic activity products, solubility product constant with respect to each calcium phosphate at 37 °C, and the number of ions in calcium phosphate, respectively. The K_{sp} values used for HA, OCP, and DCPD were 7.36×10^{-60} $(mol/L)^9$ [58], 2.51×10^{-49} $(mol/L)^8$ [59], and 2.77×10^{-7} $(mol/L)^2$ [60], respectively. The analytical results for Ca^{2+} and Pi concentrations and pH were used to calculate the IP value based on three mass balance values for Ca^{2+}, Mg^{2+}, and Pi ions [61, 62] at an ion strength of I = 150 mM. In the calculations, the presence of HCO_3^- and ion pairs of $CaH_2PO_4^+$, $CaHPO_4^+$, $MgHPO_4^+$, $CaHCO_3^+$, and $MgHCO_3^+$ were assumed in the supernatants. The DS values (1.0, <1.0, and >1.0) indicated saturation, undersaturation, and supersaturation, respectively.

2.2.5 Fourier transform infrared spectroscopic (FTIR) analysis of SDF-1-loading OCP and CDHA after the incubations in the cell culture media

The chemical structures of OCP and CDHA loaded with SDF-1 before and after incubation in the culture media were analyzed using Fourier transform infrared spectroscopy (FTIR, FT/IR-6300, JASCO Corporation, Tokyo, Japan). The incubated granules were washed thrice with ultra-pure water and frozen at −20 °C for 24 h. The frozen specimens were lyophilized for 48 h. FTIR spectra of specimens were measured using the KBr method over the range of 1800–400 cm^{-1} with a resolution of 4 cm^{-1}.

2.3 Animal experiments

2.3.1 Implantation of OCP/SDF-1 in a rat femur defect

Twelve-week-old male Sprague-Dawley rats (Japan SLC Inc. Hamamatsu, Japan) were used for animal experiments in this study. The bone formation and degradation of OCP loaded with different amounts of SDF-1 were examined in a standardized rat femur defect model. All experiments followed the principles of standard laboratory animal care and national laws. All animal handling and treatment protocols were approved by the Animal Research Committee of Tohoku University (approval number: 2021DnA-029-01). The rats were anesthetized by an intraperitoneal injection of 0.375 mg/kg medetomidine (ZENOAQ, Koriyama, Japan) and 2.5 mg/kg butorphanol (Meiji Animal Health Co., Tokyo, Japan) according to the body weight of the animals after anesthesia induction with isoflurane (MSD Animal Health, Tokyo, Japan). A standardized bone defect (3.0 mm in diameter, 3.0 mm in depth) at the lateral center of the left femur was created using a trephine drill. The bone cavity was continuously flushed with sterile saline to remove debris. The femur defects were filled with 5.0 mg of OCP/0.5 μg SDF-1 ($n = 5$), OCP/1.0 μg SDF-1 ($n = 5$), OCP/5.0 μg SDF-1 ($n = 5$), OCP without SDF-1 ($n = 5$). Although there were almost no fractures observed in the experiments, there were rare cases in which they occurred, and in such cases, additional experiments were conducted to ensure the number of experiments. Animals were sacrificed by isoflurane overdose, and femurs were collected at 2 and 4 weeks after implantation.

2.3.2 Microfocus X-ray computed tomography (Micro-CT) analysis

The collected femurs with implantation of OCP/SDF-1 and OCP were observed using a microfocus X-ray computed tomography (micro-CT) system (Scan XmateE090, Comscantecno Co., Ltd., Kanagawa, Japan) operating at 80 kV and 95 μA. Micro-CT images were analyzed using three-dimensional image analysis software (Tri-3D Bone, Ratoc, Tokyo, Japan) to measure the volumes of new bone and remaining OCP granules. The defect with a diameter of 3.0 mm and height of 3.0 mm was determined as a region of interest (ROI) in the coronal section image aligned with images of sagittal and horizontal sections. We also evaluated bone mineral density in the bone defect area using 3-dimensional reconstructed models.

2.3.3 Tissue preparation and histological analysis

The collected femur tissues were fixed with 10% paraformaldehyde for 72 h and then decalcified in a 10% EDTA

solution at pH 7.1 and 4 °C for 4 weeks. The tissues were treated with a graded series of ethanol solutions for dehydration and embedded in paraffin. The femur region, including the defect center, was sectioned into 3 μm thick slices. The sections were stained with hematoxylin and eosin (HE). The defect regions treated with OCP/SDF-1 and OCP were observed using a virtual slide scanner (NanoZoomer®, Hamamatsu Photonics K.K., Hamamatsu, Japan). The rates of newly formed bone and remaining implants in the defect region were calculated using Eqs. (4) and (5), respectively.

$$\mathrm{n-bone}(\%) = \frac{\text{newly formed bone area}(\mathrm{mm}^2)}{\text{original bone defect area}(\mathrm{mm}^2)} \times 100 \tag{4}$$

$$\mathrm{r-implant}(\%) = \frac{\text{remaining OCP area}(\mathrm{mm}^2)}{\text{original bone defect area}(\mathrm{mm}^2)} \times 100 \tag{5}$$

2.3.4 Tartrate-resistant acid phosphatase staining (TRAP)

Tissue sections were deparaffinized and then stained with a tartrate-resistant acid phosphatase (TRAP)/alkaline phosphatase staining kit (Fujifilm Wako Pure Chemical Co.) for TRAP and cell nuclei. The stained sections were imaged using an optical microscope. The number of TRAP-positive multinucleated giant cells in the ROI within the defect area or surrounding the remaining OCP granules was quantified using ImageJ 1.54i software (National Institutes of Health, Maryland, USA).

2.3.5 C-X-C motif chemokine receptor 4 (CXCR4) immunostaining

Expression of C-X-C motif chemokine receptor 4 (CXCR4), a specific receptor for SDF-1, was evaluated using immunostaining. After CXCR4 immunostaining, the number of CXCR4-positive cells per unit area in each section was counted. The sections were treated with proteinase K (Dako, California, USA) to expose the antigen, followed by an overnight incubation at 4 °C with a primary antibody specific to CXCR4 (Clone: UMB2, Anti-Rat CXCR4, Monoclonal, Abcam, Cambridge, UK). To quench the endogenous peroxidase activity, the sections were exposed to 1% hydrogen peroxide in ethanol for 20 min. This was followed by incubation with a peroxidase-labeled rat tissue secondary antibody (N-Histofine Simple Stain Rat MAX PO(M); Nichirei Bioscience Inc., Tokyo, Japan). The tissues were stained with 3,3′-diaminobenzidine tetrahydrochloride (DAB Reagent Set, Kirkegard and Perry Laboratories Inc., MD, USA) and counterstained with hematoxylin. Optical microscopy images of the sections were obtained, and CXCR4-positive cells within the ROI were quantified for histomorphometric analysis.

2.3.6 Osteocalcin immunostaining

The number of osteocalcin-positive osteoblastic cells (/mm^2) within the defects treated with OCP and OCP/SDF-1 was quantified using osteocalcin immunostaining, as previously described [63, 64]. Tissue sections were subjected to antigen retrieval with proteinase K (Dako) and incubated overnight at 4 °C with a monoclonal antibody specific to rat osteocalcin (Clone 6-7H, Takara Bio Inc). Following the primary antibody reaction, endogenous peroxidase activity was inhibited by treating the tissues with 1% H_2O_2 in ethanol for 20 min. Subsequently, a secondary antibody reaction was performed using a peroxidase-labeled rat-specific secondary antibody (N-Histofine Simple Stain Rat MAX PO(M), Nichirei Bioscience Inc). The reaction was visualized using 3,3′-diaminobenzidine tetrahydrochloride (DAB Reagent Set, Kirkegard and Perry Laboratories Inc), and the sections were counterstained with hematoxylin. Immunostained sections were imaged using a digital slide scanner (NanoZoomer-SQ, Hamamatsu Photonics K.K.).

For quantitative analysis, one section per animal from each treatment group was evaluated at 2 and 4 weeks post-implantation. Images were acquired from a field of view encompassing the entire defect region. The number of osteocalcin-positive cells was quantified per unit area within the region of interest (a 3-mm-wide defect area) based on the scanned images.

2.4 Statistical analysis

Results are expressed as mean ± standard deviation. One-way analysis of variance with a post hoc Tukey-Kramer test was used to examine statistical differences. Statistical analyses were performed using data analysis software (JMP version 17.1; SAS, Cary, NC, USA). Differences were considered statistically significant at $p < 0.05$.

3 Results

3.1 Microstructure of SDF-1-loaded OCP and CDHA granules

Figure 1 shows the SEM images of OCP and CDHA granules before and after the loading of SDF-1. The aggregation of plate-like crystals toward the long axis was observed in the OCP and CDHA granules. The width of the plate-like crystals tended to be smaller for CDHA than for

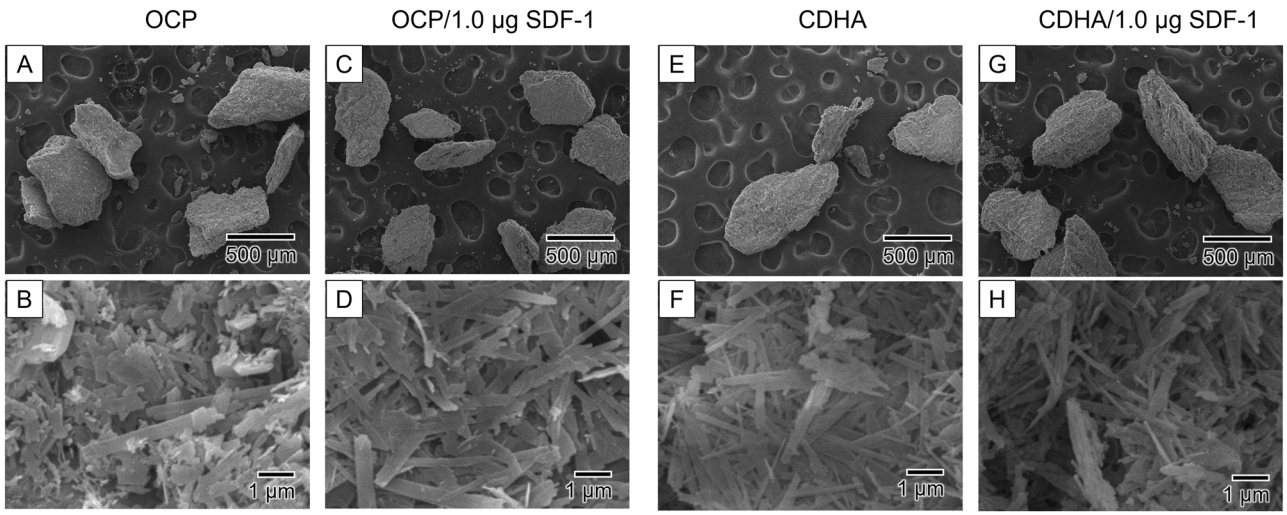

Fig. 1 SEM images of OCP (**A**, **B**), OCP/1.0 μg SDF-1 (**C**, **D**), CDHA (**E**, **F**), and CDHA/1.0 μg SDF-1 (**G**, **H**) at lower (**A**, **C**, **E**, **G**) and higher magnifications (**B**, **D**, **F**, **H**). Bars = 500 μm (**A**, **C**, **E**, **G**) and 1 μm (**B**, **D**, **F**, **H**)

OCP. The granular form and crystal morphology of OCP and CDHA were maintained after the process of SDF-1 loading.

3.2 MSC migration to OCP/SDF-1 and CDHA/SDF-1 in vitro

Figure 2A shows the rate of MSC migration toward OCP/SDF-1 and CDHA/SDF-1 cells in vitro at 48 h. The migration rates of MSCs in the OCP/SDF-1 and OCP groups were higher than in the control and 1.0 μg SDF-1 groups. The migration rates in the CDHA and CDHA/1.0 μg SDF-1 were also significantly higher than in the control group. In addition, the migration rate for the OCP and CDHA groups tended to increase compared with the 1.0 μg SDF-1 group.

A significant difference was observed between the control and the OCP or OCP/SDF-1 groups. The migration rate increased with increasing SDF-1 loading in the OCP range of 0–1.0 μg. However, the migration rate in the OCP/5.0 μg SDF-1 decreased compared with other OCP/SDF-1 groups. A significant difference was observed between the 1.0 μg SDF-1 and OCP/1.0 μg SDF-1 groups. In addition, the OCP/1.0 μg SDF-1 rate tended to be higher than in the CDHA/1.0 μg SDF-1.

3.3 SDF-1 concentrations in cell culture media incubated with OCP/SDF-1 and CDHA/SDF-1

Figure 2B shows the changes in SDF-1 concentrations in the culture media after OCP/SDF-1 and CDHA/SDF-1 incubation for 3, 6, 24, and 48 h. The concentration of SDF-1 in the medium incubated with OCP/SDF-1 increased with the increase of the incubation period up to 24 h and then decreased at 48 h. The concentration in the 1.0 μg SDF-1 group was higher than in the CDHA/1.0 μg SDF-1 and OCP/0.5 and 1.0 μg SDF-1 groups at 3 h. However, the concentration for the 1.0 μg SDF-1 group decreased with the increase of the incubation periods. The SDF-1 concentration in the OCP/5.0 μg SDF-1 drastically increased compared with the other OCP/SDF-1 groups at 3 h. At 3 h, the SDF-1 concentration in the OCP/1.0 μg SDF-1 group was higher than in the OCP/0.5 μg SDF-1 group. The order of SDF-1 concentrations in the OCP/SDF-1 groups at 3 h was maintained until 48 h. Furthermore, the concentration of SDF-1 in the CDHA/1.0 μg SDF-1 group tended to be higher than in the OCP/1.0 μg SDF-1 at 3 h and 6 h. After incubation for 24 and 48 h, these groups showed similar concentrations in the culture media.

Figure 2D shows the changes in SDF-1 release rates of OCP/SDF-1 and CDHA/SDF-1 during incubation in cell culture media. The SDF-1 release rate for all OCP/SDF-1 groups slightly increased from 0 to 24 h; however, the rate for the CDHA/1.0 μg SDF-1 group increased from 0 to 3 h and then was maintained. The release rate of the OCP/SDF-1 group increased with the amount of SDF-1 loaded onto the granules during each incubation period. The release rate for the CDHA/1.0 μg SDF-1 was higher than that for the OCP/1.0 μg SDF-1 group at 3 and 6 h, and the release rates for these groups were similar from 24 to 48 h.

3.4 Adsorption analysis

Figure 2E shows the SDF-1 adsorption isotherms of OCP and CDHA in 100 mM HEPES- 50 mM NaCl buffer, saturated and supersaturated with respect to OCP and HA,

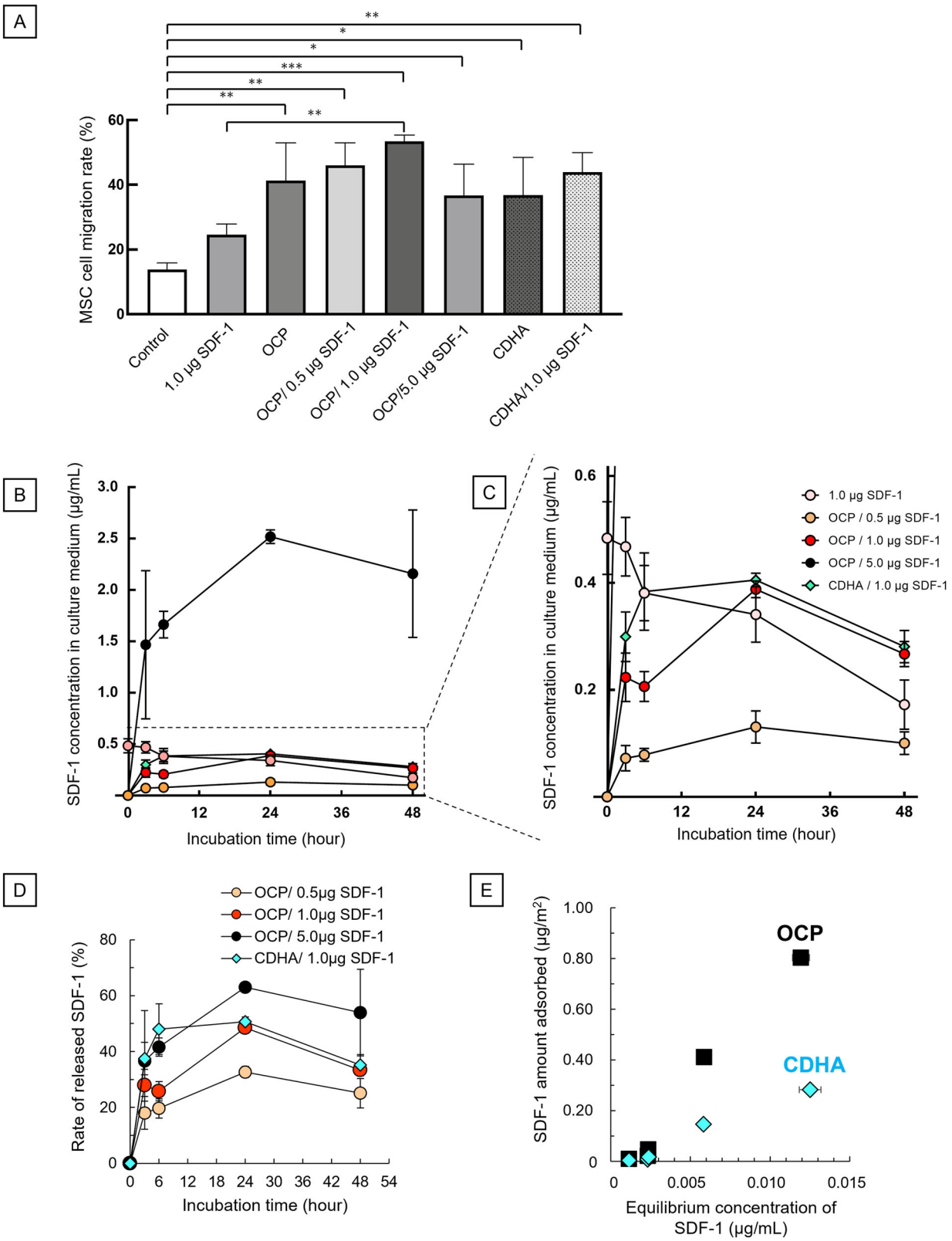

respectively. The amounts adsorbed onto OCP and CDHA increased with increasing equilibrium concentrations. The amount of adsorbed onto OCP was larger than that onto CDHA, ranging from 0.0025 to 0.012 μg/mL. The adsorption isotherms of SDF-1 onto OCP and CDHA were approximated using the Freundlich adsorption isotherm

◀ **Fig. 2** Migration rates of mouse bone marrow-derived MSCs cultured in the presence of 1.0 μg SDF-1, OCP/SDF-1 (0, 0.5, 1.0, and 5.0 μg), and CDHA/SDF-1 (0 and 1.0 μg) granules at 48 h (*$p < 0.05$, **$p < 0.01$, ***$p < 0.001$) (**A**). Changes in SDF-1 concentration in cell culture media incubated with 1.0 μg SDF-1, OCP/SDF-1, and CDHA/SDF-1 at 3, 6, 24, and 48 h (**B**). The region with a broken line indicates the area shown as a magnified graph in Fig. 2C. Magnified graph of changes in SDF-1 concentration in the culture media (**C**). SDF-1 release rates of OCP and CDHA granules in culture media at 3, 6, 24, and 48 h (**D**). Adsorption isotherms of SDF-1 onto OCP and CDHA plotted as adsorption amount per unit surface area of OCP and CDHA, respectively, as a function of SDF-1 equilibrium concentration in the 100 mM HEPES-50 mM NaCl buffer containing 0.5 mM Ca^{2+} and 0.5 mM Pi ion at pH 7.4 and 37 °C (**E**)

equation to calculate the adsorption parameters (Table 1). The correlation coefficients for OCP and CDHA indicate that the isotherms obtained in the adsorption tests fit the Freundlich equation well. The calculated 1/n values were similar for OCP and CDHA. However, the value of K_f for the OCP was higher than that for CDHA.

3.5 Ion concentrations and DS with respect to calcium phosphates in culture media

Table 2 shows the ion composition of the cell culture medium before and after incubation with OCP/SDF-1 and CDHA/SDF-1 for 48 h. Ca^{2+} concentration decreased after incubation with OCP/SDF-1 and CDHA/SDF-1. The Ca^{2+} concentrations in the OCP and OCP/SDF-1 groups were higher than in the CDHA and CDHA/1.0 μg SDF-1 groups. Although the Pi ion concentrations in the media incubated with CDHA and CDHA/SDF-1 decreased, those in the media incubated with OCP and OCP/SDF-1 increased slightly. The pH values of culture media were ~7.8 after incubation with OCP and CDHA, regardless of the amount of SDF-1 loaded.

The calculated DS values with respect to calcium phosphates in the culture medium before and after incubation with OCP and CDHA granules loaded with different amounts of SDF-1 are shown in Table 2. DS with respect to DCPD suggested that all culture media were undersaturated with respect to DCPD. The DS values indicated that the culture media were supersaturated with respect to HA and OCP after incubation with OCP and OCP/SDF-1 granules for 48 h. The DS values with respect to HA were higher than those with respect to OCP in culture media in the presence of OCP and OCP/SDF-1 granules. The DS values also indicated that the culture media were supersaturated with respect to HA and undersaturated with respect to OCP after incubation with CDHA and CDHA/SDF-1 granules. The DS value with respect to HA and OCP increased in the CDHA/1.0 μg SDF-1 group compared with the CDHA group at 48 h. However, the DS with respect to HA and OCP decreased in the OCP/1.0 μg SDF-1 group compared with the OCP group.

Table 1 Parameters of SDF-1 adsorption onto OCP and CDHA estimated by approximating the adsorption isotherms to Freundlich's isotherm equation

Adsorbents	K_f	1/n	R^2
OCP	7413	2.01	0.948
CDHA	2238	1.99	0.946

3.6 FTIR analysis of OCP/SDF-1 and CDHA/SDF-1 incubated in the culture media

Figure 3 shows the FTIR spectra of OCP/SDF-1 and CDHA/SDF-1 before and after incubation in cell culture media for 48 h. The bands of ν_4 PO_4 were detected at 560 and 600 cm^{-1} in the OCP and OCP/SDF-1 spectra before incubation. The bands attributed to ν_3 PO_4 and ν_3 PO_4/HPO_4 appeared in these spectra at 1023 and 1060 cm^{-1}, respectively. The bands corresponding to ν_3 HPO_4 (5) and ν_3 HPO_4 (6) were detected at 1103 and 1124 cm^{-1}, respectively. After the incubations at 48 h, the intensities of bands attributed to ν_3 HPO_4 (5) and ν_3 HPO_4 (6) decreased in the OCP and OCP/SDF-1 spectra regardless of the loading amount of SDF-1. However, the intensities of ν_3 HPO_4 (5) and ν_3 HPO_4 (6) tended to be higher in the OCP/5.0 μg SDF-1 than in the OCP/1.0 μg SDF-1 and OCP/0.5 μg SDF-1 after the incubations. In the CDHA and CDHA/SDF-1 spectra, bands of ν_4 PO_4 were detected at 560 and 600 cm^{-1}, and the band attributed to OH was observed at 630 cm^{-1}. The bands corresponding to ν_3 PO_4 and ν_3 HPO_4 appeared in these spectra at 1028 and 1090 cm^{-1}. The characteristic bands attributed to CDHA were maintained after incubation with or without SDF-1 loading. After immersion in OCP and CDHA, regardless of the amount of SDF-1 loading, bands corresponding to amide I and II were detected at 1650 and 1540 cm^{-1}, respectively.

3.7 Micro-CT analysis of rat femur defects implanted with OCP/SDF-1 granules

Figure 4 shows the micro-CT images of the sagittal sections of the bone defect after OCP/SDF-1 granule implantation at 2 and 4 weeks. The radiopaque regions with granular shape were observed in both intramural and cortical bone areas in the defect region after the OCP, OCP/0.5 μg SDF-1 implantation, and OCP/5.0 μg SDF-1 at 2 weeks. However, granular radiopaque areas seemed to be blurred, and radiopaque intensity tended to be higher in the OCP/1.0 μg SDF-1 group at 2 weeks. The granular radiopaque regions in the intramedullary bone region decreased, and the radiopaque intensity in the cortical bone region increased at 4 weeks compared to 2 weeks, regardless of the amount of SDF-1 loaded on the OCP granules. At 4 weeks, the remaining granular radiopaque areas seemed smaller in the OCP/1.0 μg SDF-1 group than in the other groups.

Table 2 Solution composition and degree of supersaturation (DS) of culture media incubated with OCP and CDHA loaded with different amounts of SDF-1

Supernatants	Incubation periods (hour)	Ca (mM)	Pi (mM)	pH	DS at 37 °C		
					HA	OCP	DCPD
Culture medium	0	1.78	1.11	7.35	2.88×10^{11}	1.13×10^{3}	5.99×10^{-1}
Culture medium	48	2.06	1.09	7.86	9.15×10^{13}	2.99×10^{4}	7.78×10^{-1}
OCP	48	0.53	1.16	7.81	9.15×10^{10}	1.46×10^{2}	2.24×10^{-1}
OCP/0.5 μg SDF-1	48	0.49	1.23	7.83	8.88×10^{10}	1.40×10^{2}	2.20×10^{-1}
OCP/1.0 μg SDF-1	48	0.48	1.25	7.83	8.39×10^{10}	1.35×10^{2}	2.19×10^{-1}
OCP/5.0 μg SDF-1	48	0.49	1.26	7.83	9.50×10^{10}	1.50×10^{2}	2.25×10^{-1}
CDHA	48	0.18	0.69	7.85	1.47×10^{8}	5.65×10^{-1}	4.71×10^{-2}
CDHA/1.0 μg SDF-1	48	0.20	0.68	7.86	2.63×10^{8}	8.67×10^{-1}	5.17×10^{-2}

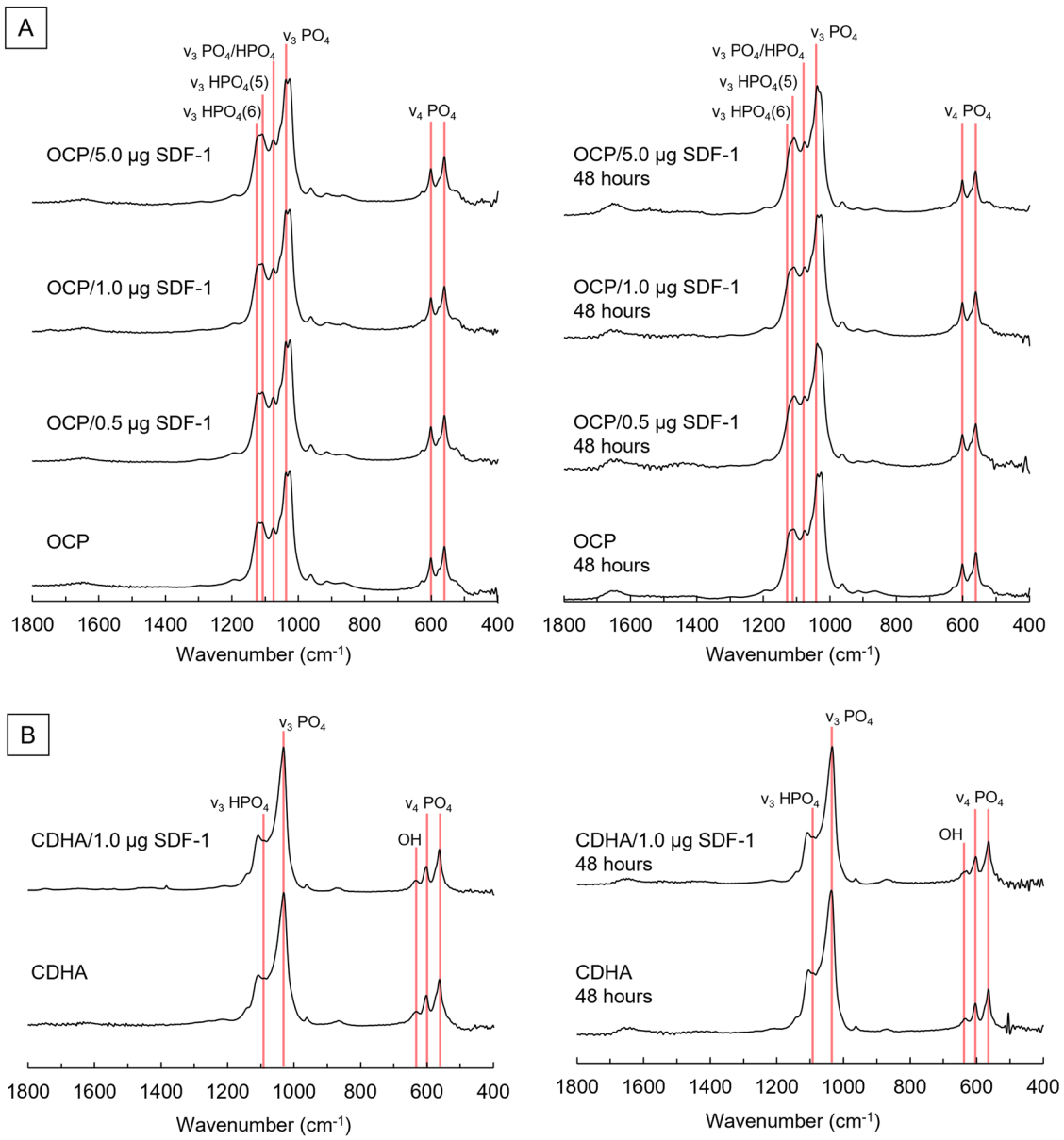

Fig. 3 FTIR spectra of OCP (**A**) and CDHA (**B**) granules loaded with different amounts of SDF-1 before and after incubations in culture media at 48 h

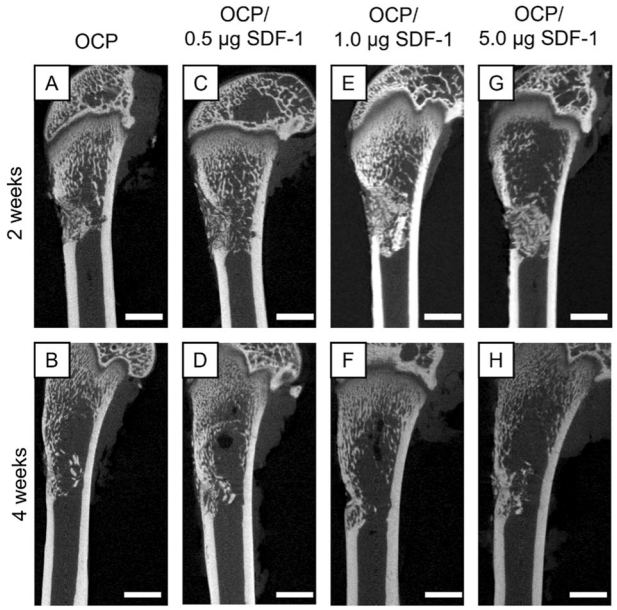

Fig. 4 Micro-CT images of the rat femur around the region of defects treated with OCP (**A**, **B**), OCP/0.5 μg SDF-1 (**C**, **D**), OCP/1.0 μg SDF-1 (**E**, **F**), and OCP/5.0 μg SDF-1 (**G**, **H**) at 2 weeks (**A**, **C**, **E**, **G**) and 4 weeks (**B**, **D**, **F**, **H**) post-implantation. Bars in images represent 2.5 mm

3.8 Quantitative analyses of new bone and remaining OCP in rat femur defects implanted with OCP/SDF-1 granules

Figure 5 shows the new bone and remaining OCP volumes in the ROI estimated using micro-CT image analysis. At 2 weeks, the new bone volume significantly increased in the OCP/1.0 μg SDF-1 group compared with the OCP and OCP/0.5 μg SDF-1 groups. The bone volume in the OCP/1.0 μg SDF-1 group was larger than that in the OCP/5.0 μg SDF-1 group; however, there was no significant difference. The bone volume in the OCP, OCP/0.5 μg SDF-1, and OCP/5.0 μg SDF-1 at 4 weeks was compared with 2 weeks. However, the volume tended to decrease in the OCP/1.0 μg SDF-1 group and became comparable to the OCP/5.0 μg SDF-1 group with no significant difference at 4 weeks. The volume of new bone was slightly larger in the OCP/1.0 μg SDF-1 group than in the other groups at 4 weeks.

The volume of the remaining OCP granules in the OCP/1.0 μg SDF-1 group was the smallest among all groups at 2 weeks. A significant difference was observed between the OCP/1.0 μg SDF-1 group and the OCP or OCP/0.5 μg SDF-1 group. The remaining OCP decreased in all groups from 2 to 4 weeks. The remaining OCP volume was smaller in the OCP/1.0 μg SDF-1 group than in the other groups. There was a significant difference between the OCP/1.0 μg SDF-1 and OCP groups. The remaining volume in the OCP/0.5 μg SDF-1 and OCP/5.0 μg SDF-1 groups tended to decrease compared with that in the OCP group at 4 weeks; however, there was no significant difference.

The BMD in the OCP/SDF-1 1.0 μg group was 600 ± 35.6 mg/cm³, which was significantly higher than that in the OCP/SDF-1 5.0 μg group (527.4 ± 30.0 mg/cm³) and the OCP group (537.2 ± 31.7 mg/cm³). However, there was no significant difference compared to the OCP/SDF-1 0.5 μg group (552.3 ± 30.0 mg/cm³). To enhance visual assessment of new bone formation, 3-dimensional reconstructed CT models were also evaluated. Among the groups, the OCP/SDF-1 1.0 μg group at 2 weeks exhibited a significant enhancement in bone formation compared to the others. In contrast, the BMD at 4 weeks showed no significant differences among the groups.

3.9 Histological analysis of rat femur defects implanted with OCP/SDF-1 granules

Figures 6 and 7 show the histological images of HE staining of rat femur defects after OCP/SDF-1 granule implantation at lower and higher magnifications, respectively. At 2 weeks, newly formed bone was observed in the intramedullary bone regions in the bone defects in all groups. The newly formed bone tissues directly contacted the OCP granules, regardless of the amount of SDF-1. Although OCP granules remained over the entire region of the defect in the OCP, OCP/0.5 μg SDF-1, and OCP/5.0 μg SDF-1 groups at 2 weeks, the amount of the remaining OCP granules seemed to be smaller and replaced with new bone in the OCP/1.0 μg SDF-1 group.

At 4 weeks, new bone tissue bridged the edges of the bone defects in the cortical bone regions in all groups. The new bone tissue and remaining OCP granules were resorbed in the intramedullary bone regions of the defects. However, the new bone amount and remaining amount of OCP in the intramedullary bone seemed to be smaller in the OCP/1.0 SDF-1 group than in the other groups. Furthermore, the replacement of OCP granules with new bone in the cortical bone region progressed in the OCP/1.0 SDF-1 compared to other groups at 4 weeks.

3.10 Histomorphometric analysis

Figure 8 shows the quantitative values of the newly formed bone and remaining OCP granule rate in the defects treated with OCP/SDF-1 at 2 and 4 weeks. The rate of newly formed bone (n-bone (%)) in the OCP/1.0 μg SDF-1 group showed the highest value among all groups at 2 weeks with significant differences. The n-bone (%) values were similar among the OCP, OCP/0.5 μg SDF-1, and OCP/5.0 μg SDF-1 groups. The n-bone (%) tended to increase in the OCP, OCP/0.5 μg SDF-1, and OCP/5.0 μg SDF-1 groups from 2 to 4 weeks; however, the values of n-bone (%) were maintained in the OCP/1.0 μg SDF-1 groups at 4 weeks. The n-bone (%) was also higher in the OCP/1.0 μg SDF-1

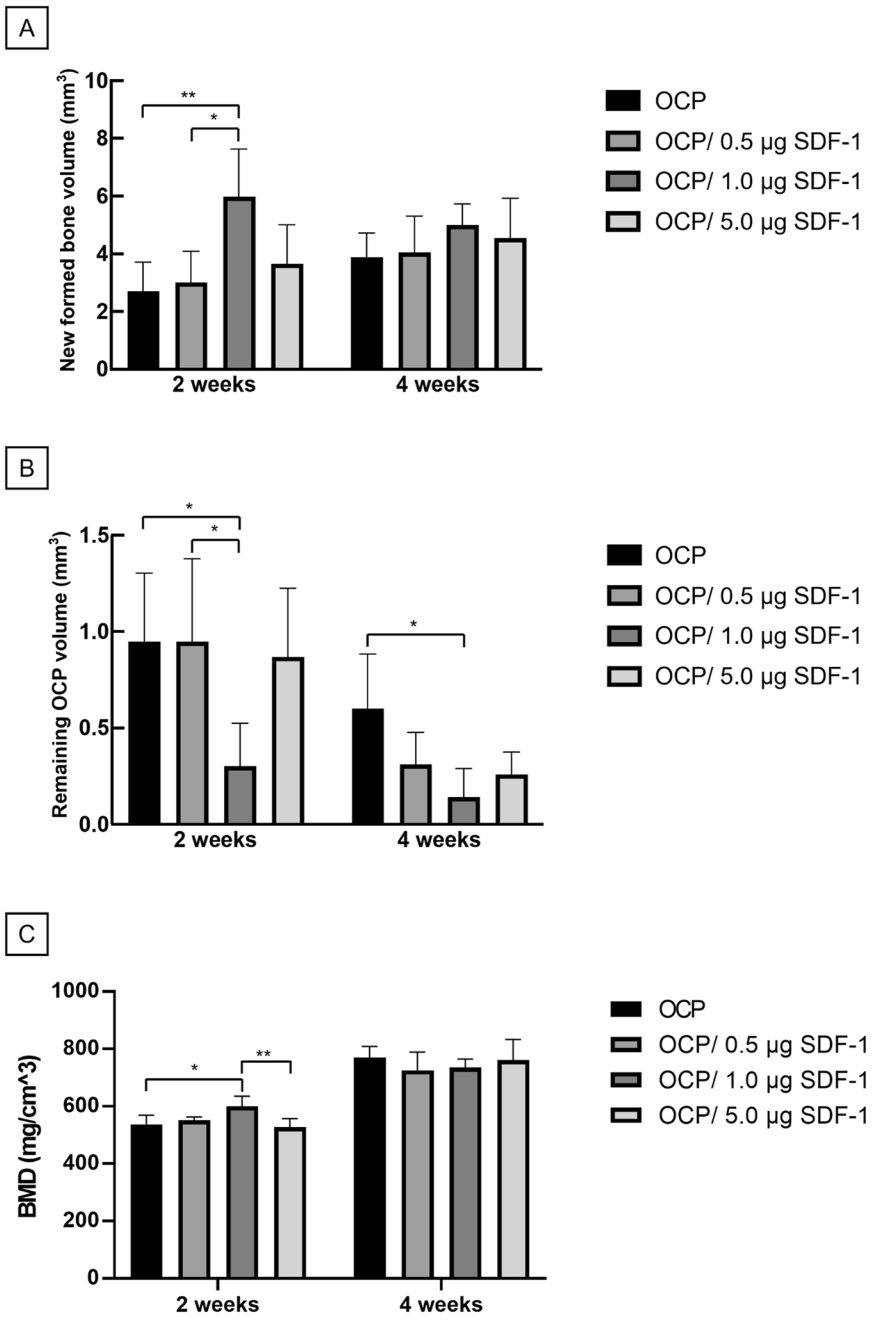

Fig. 5 Quantitative analysis using micro-CT of new bone volume (**A**), remaining OCP volume (**B**), and bone mineral density in 3-dimensional reconstructed models (**C**) in ROI of rat femur bone defects treated with OCP, OCP/0.5 μg SDF-1, OCP/1.0 μg SDF-1, and OCP/5.0 μg SDF-1 at 2 and 4 weeks. (*$p < 0.05$, **$p < 0.01$)

group than in the other groups at 4 weeks. However, this difference was not statistically significant.

The rate of the remaining OCP granules (r-implant (%)) in the OCP/1.0 μg SDF-1 group had the lowest value among all groups at 2 weeks with significant differences. The r-implant (%) values tended to be higher in the OCP/5.0 μg SDF-1 group than in the OCP and OCP/0.5 μg SDF-1 groups at 2 weeks. At 4 weeks, r-implant (%) decreased in all groups, and the value was significantly lower in the OCP/1.0 μg SDF-1 group than in the OCP and OCP/0.5 μg SDF-1 groups. The r-implant (%) for the OCP/1.0 μg SDF-1 group also decreased compared with the OCP/5.0 μg SDF-1 group at 4 weeks; however, a significant difference was not observed. The r-implant (%) values in the OCP/5.0 μg SDF-1 group tended to be lower than in the OCP and OCP/0.5 μg SDF-1 groups.

3.11 TRAP staining analysis

TRAP staining of osteoclast-like cells showed an increased count of TRAP-positive cells in the OCP/1.0 μg SDF-1 group compared with the OCP, OCP/0.5 μg SDF-1, and OCP/5.0 μg SDF-1 at both 2 and 4 weeks (Fig. 9A–H, I–P). TRAP-positive multinucleated cells were predominantly expressed

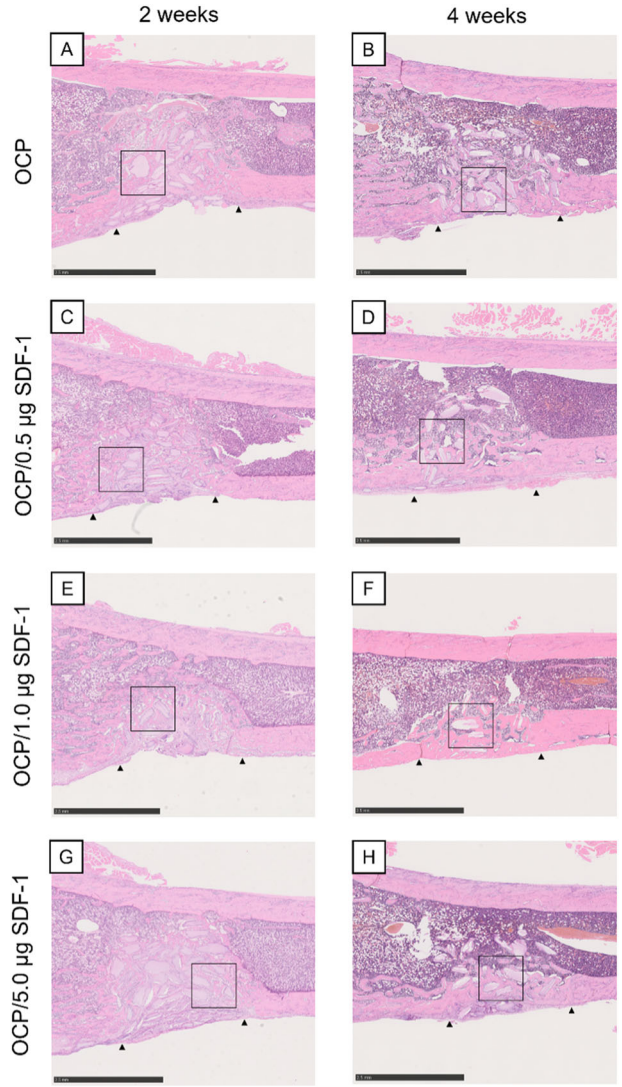

Fig. 6 Overview of histological sections stained with hematoxylin and eosin around the region of rat femur defects treated with OCP (**A**, **B**), OCP/0.5 μg SDF-1 (**C**, **D**), OCP/1.0 μg SDF-1 (**E**, **F**), and OCP/5.0 μg SDF-1 (**G**, **H**) at 2 weeks (**A**, **C**, **E**, **G**) and 4 weeks (**B**, **D**, **F**, **H**) post-implantation. The arrowheads indicate the edges of the bone defects. The open squares indicate the areas shown as higher magnified images in Fig. 7. Bars in images represent 2.5 mm

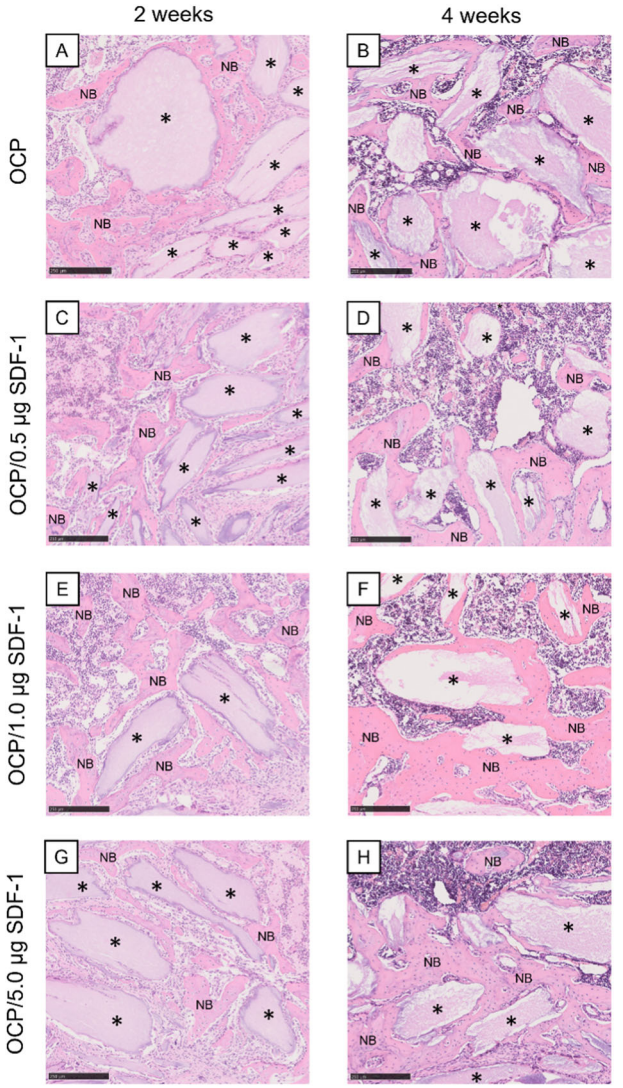

Fig. 7 Higher magnified images of histological sections stained with hematoxylin and eosin in the region of rat femur defects treated with OCP (**A**, **B**), OCP/0.5 μg SDF-1 (**C**, **D**), OCP/1.0 μg SDF-1 (**E**, **F**), and OCP/5.0 μg SDF-1 (**G**, **H**) at 2 weeks (**A**, **C**, **E**, **G**) and 4 weeks (**B**, **D**, **F**, **H**) post-implantation. NB and asterisks indicate the newly formed bone and remaining OCP granules, respectively. Bars in images represent 250 μm

around the residual granules of OCPs and the surrounding new bone. TRAP-positive multinucleated cells were measured in the ROI of the defect region at 2 and 4 weeks (Fig. 9Q). At week 4, there was a higher count of TRAP-positive multinucleated cells compared with week 2 across all groups. At week 2, the count of TRAP-positive multinucleated cells was significantly higher in the OCP/0.5 μg SDF-1, OCP/1.0 μg SDF-1, and OCP/5.0 μg SDF-1 groups compared with the OCP alone group; the respective counts (cells/mm^2) for the OCP, OCP/0.5 μg SDF-1, OCP/1.0 μg SDF-1, and OCP/5.0 μg SDF-1 groups were 1.5 ± 0.2, 2.6 ± 0.8, 3.3 ± 0.5, and 2.6 ± 0.3. At week 4, the count of TRAP-positive cells in the OCP/1.0 μg SDF-1 group was significantly greater than in OCP alone or other SDF-1-loaded OCP with varying concentrations of SDF-1 groups; the respective counts (cells/mm^2) for the OCP, OCP/0.5 μg SDF-1, OCP/1.0 μg SDF-1, and OCP/5.0 μg SDF-1 groups were 2.1 ± 0.5, 3.1 ± 0.7, 4.3 ± 0.6, and 2.8 ± 0.4, respectively. The OCP/1.0 μg SDF-1 concentration was the most effective for activating osteoclasts.

3.12 CXCR4 immunohistomorphometric analysis

Images of CXCR4 immunostaining at low and high magnifications are presented for 2 and 4 weeks after OCP and SDF-1-loaded OCP implantation with varying concentrations

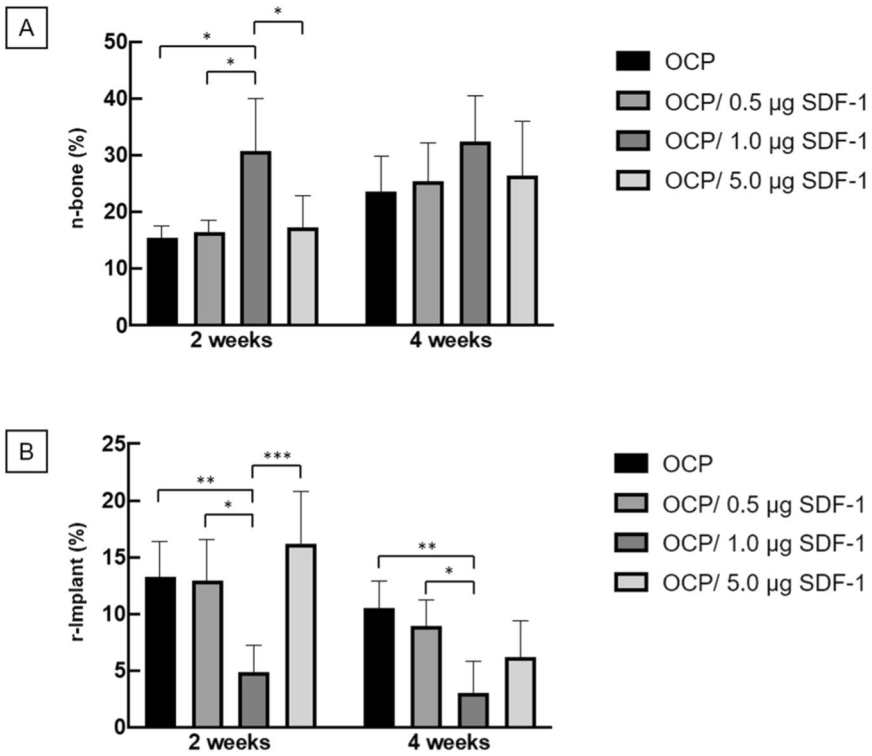

Fig. 8 Histomorphometric analysis of the newly formed bone (**A**) and remaining OCP granules (**B**) in the rat femur defect region treated with OCP, OCP/0.5 µg SDF-1, OCP/1.0 µg SDF-1, and OCP/5.0 µg SDF-1 at 2 and 4 weeks post-implantation. (*$p < 0.05$, **$p < 0.01$, ***$p < 0.001$)

of SDF-1. At 2 weeks (Fig. 10A–H), all groups exhibited CXCR4-positive cells in the marginal areas of the bone defects. In the OCP/1.0 µg SDF-1 group, CXCR4-positive cells were prominent. By week 4 (Fig. 10I–P), CXCR4-positive cells were observed in all groups around the margins of the defect, close to the new bone formation area at the center of the bone defect. Figure 10Q illustrates the counts of CXCR4-positive cells within the ROI area. At 2 weeks, the respective counts (cells/mm^2) for the OCP, OCP/0.5 µg SDF-1, OCP/1.0 µg SDF-1, and OCP/5.0 µg SDF-1 groups were 24.4 ± 4.7, 32.5 ± 7.8, 49.2 ± 5.8, and 31.4 ± 8.9, respectively. The number of CXCR4-positive cells was significantly higher in the OCP/1.0 µg SDF-1 group than in the other groups. By 4 weeks, the counts were 16.4 ± 6.5, 27.0 ± 7.2, 21.7 ± 10.6, and 14.9 ± 4.4 for the OCP, OCP/0.5 µg SDF-1, OCP/1.0 µg SDF-1, and OCP/5.0 µg SDF-1 groups, respectively. There were no significant differences among the groups. In each group, the number of CXCR4-positive cells was higher at 2 weeks than at 4 weeks. A significant increase in CXCR4-positive cells was observed in the group treated with 1.0 µg of SDF-1, suggesting an optimal concentration of SDF-1 for osteoblast differentiation and osteoclast activation.

3.13 Osteocalcin immunostaining analysis

Osteocalcin-positive cells were identified around the newly formed bone in the defect region within the OCP and OCP/SDF-1 groups at 2 and 4 weeks post-implantation (Fig. 11A–P). At 2 weeks, the number of osteocalcin-positive cells was significantly higher in the OCP/1.0 µg SDF-1 group (41.7 ± 8.3/mm^2) compared to the OCP group (21.8 ± 4.6/mm^2), OCP/0.5 µg SDF-1 group (20.1 ± 5.2/mm^2) with $p < 0.001$ for each comparison (Fig. 11Q). The osteocalcin-positive cells significantly increased in the OCP/1.0 µg SDF-1 group compared with OCP/5.0 µg SDF-1 group (27.7 ± 6.7/mm^2) ($p < 0.05$). However, by 4 weeks, the number of osteocalcin-positive cells in the OCP/1.0 µg SDF-1 group had decreased to 20.5 ± 6.5/mm^2, with no significant differences observed between the groups (Fig. 11Q).

4 Discussion

The results presented herein indicate that adding the chemokine SDF-1 synergistically enhanced bone regeneration following OCP implantation in rat femoral standardized defects (Figs. 5–8). One of the essential mechanisms is the recruitment of MSC toward OCP granules (Fig. 2A) through the function of SDF-1 [49] present on the surface of OCP. This strengthens the osteoconductive performance of OCP, which is an inherent property of OCP that promotes the differentiation of pre-osteoblasts into osteoblasts and bone formation [1, 2, 40]. The sustained release of SDF-1 from OCP (Fig. 2B–D) suggested that the molecular adsorption capacity of OCP [14] may be essential for the synergistic effect of OCP and SDF-1 on bone formation. A comparative study using CDHA as a control material also

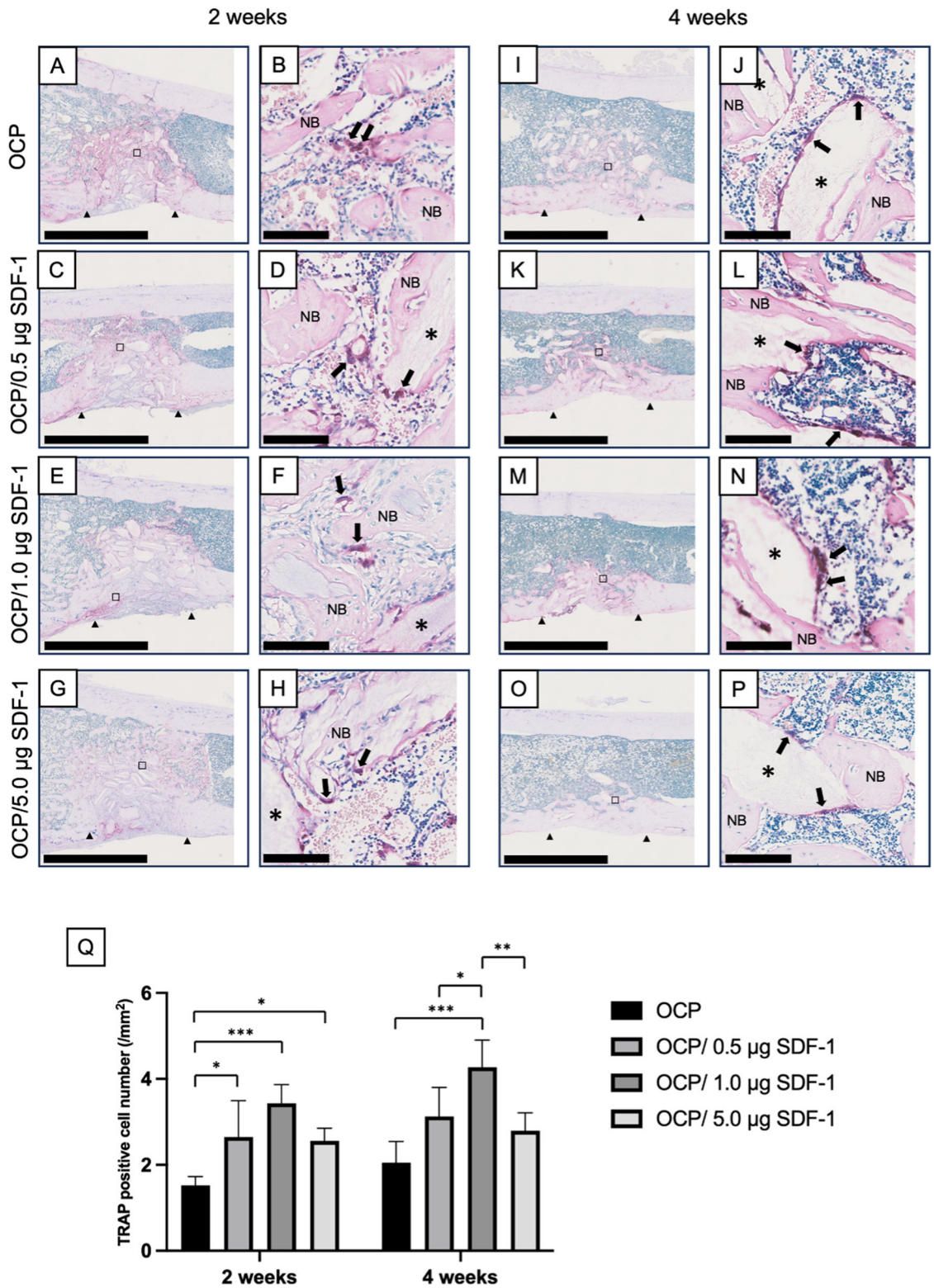

Fig. 9 Lower and higher magnified images of rat femur bone defect regions in the section with TRAP staining at 2 weeks (**A**–**H**) and 4 weeks (**I**–**P**) after implantation of OCP, OCP/0.5 μg SDF-1, OCP/1.0 μg SDF-1, and OCP/5.0 μg SDF-1. Arrowheads indicate the edges of defects. Arrows indicate TRAP-positive cells; asterisks indicate remaining OCP granules. The open squares in the lower magnified images indicate the area shown in the higher magnified images. Bars in the images at lower and higher magnification represent 2.5 mm and 100 μm, respectively. Quantitative analysis of the number of TRAP-positive cells in the ROI of the defect region (**Q**). (*$p < 0.05$, **$p < 0.01$, ***$p < 0.001$)

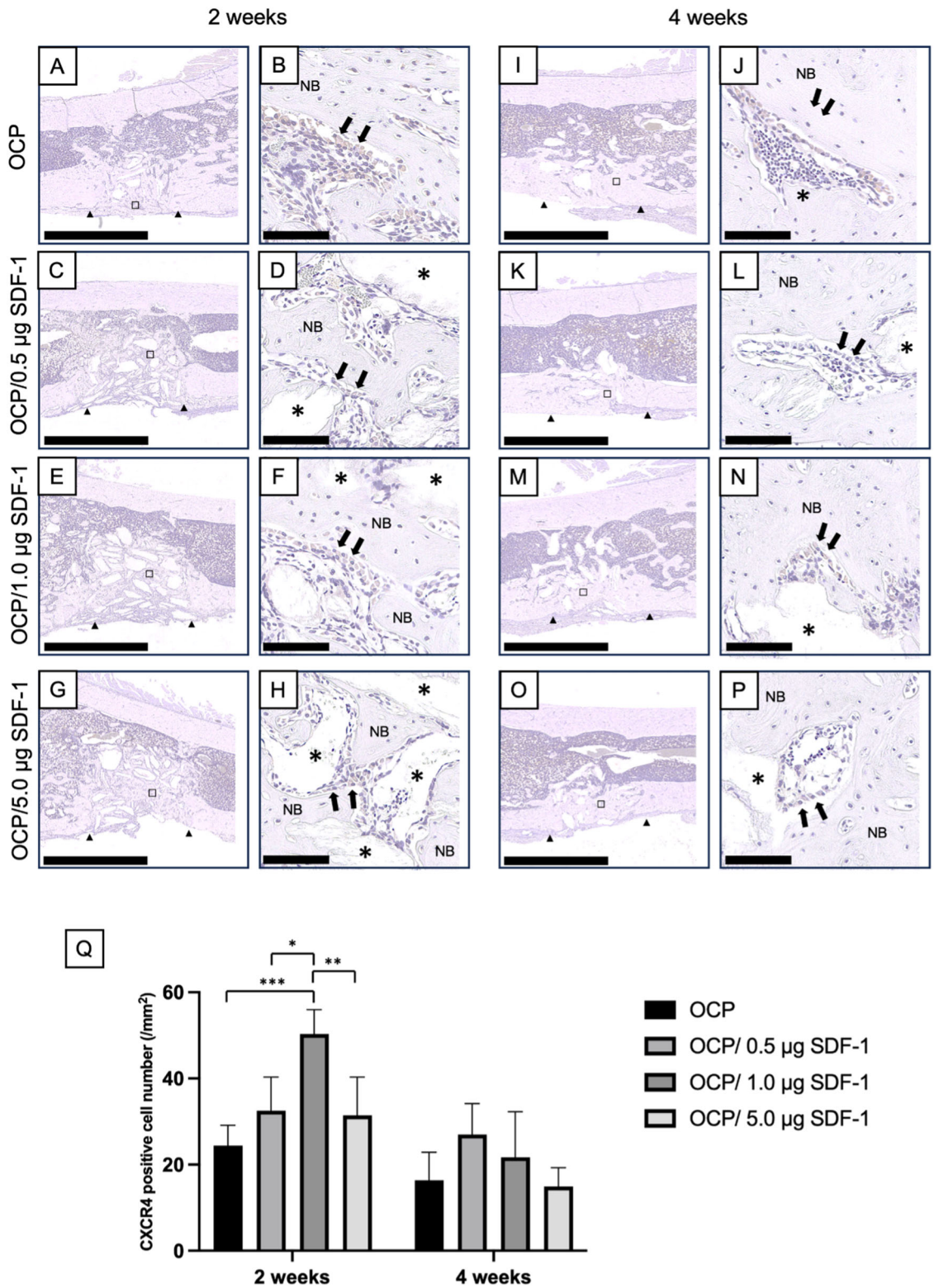

Fig. 10 Lower and higher magnified images of the rat femur bone defect regions in the section with CXCR4 immunostaining staining at 2 weeks (**A**–**H**) and 4 weeks (**I**–**P**) after implantation of OCP, OCP/0.5 μg SDF-1, OCP/1.0 μg SDF-1, and OCP/5.0 μg SDF-1. Arrowheads indicate the edges of the defects. Arrows indicate CXCR4-positive cells; asterisks indicate remaining OCP granules. The open squares in the lower magnified images indicate the area shown in the higher magnified images. Bars in the images at lower and higher magnification represent 2.5 mm and 100 μm, respectively. Quantitative analysis of the number of CXCR4-positive cells in the ROI of the defect region (**Q**). (*$p < 0.05$, **$p < 0.01$, ***$p < 0.001$)

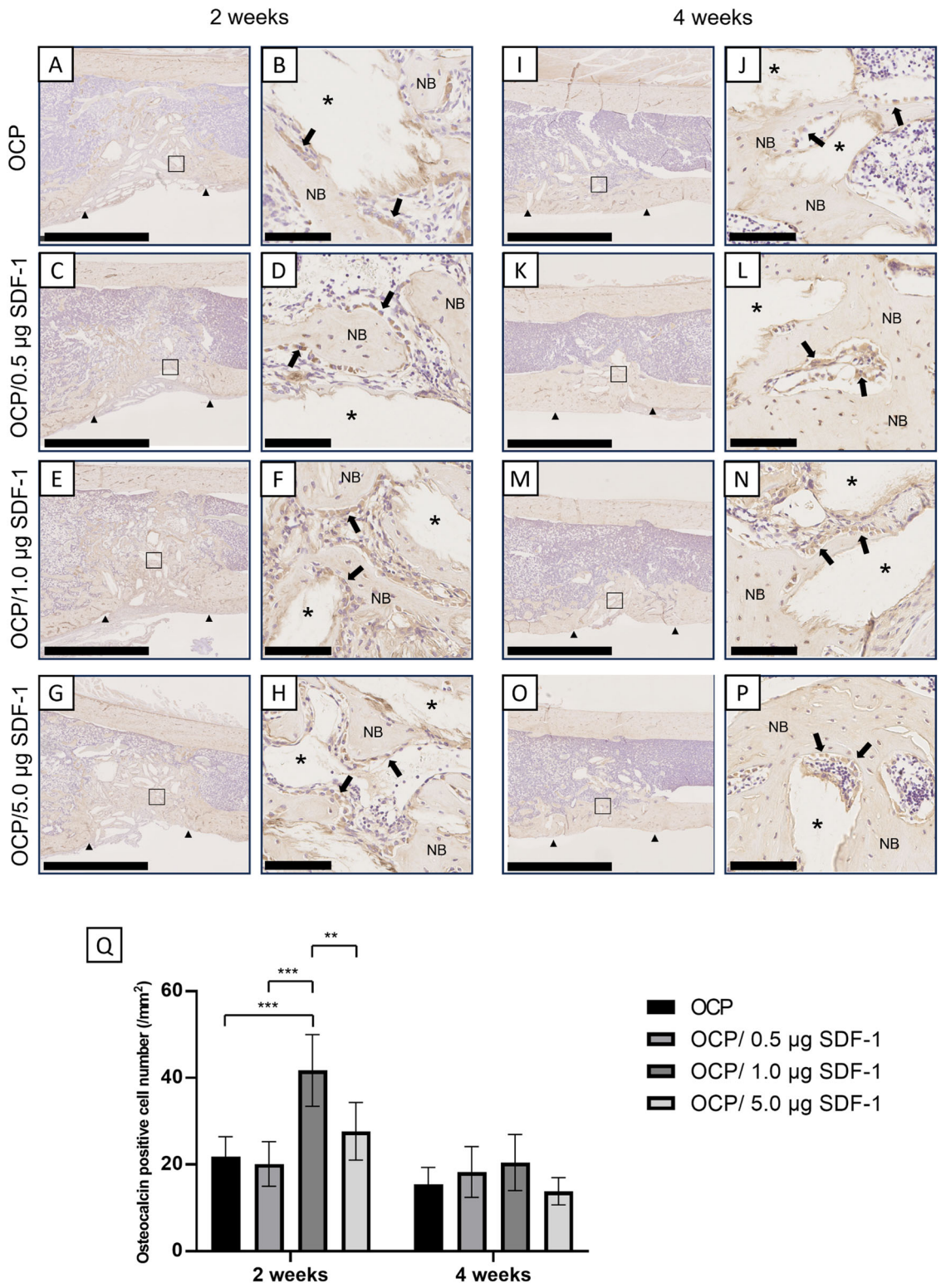

Fig. 11 Low- and high-magnification images of the osteocalcin-immunostained sections of the rat femur in the bone defect area at 2 weeks (**A**–**H**) and 4 weeks (**I**–**P**) after implantation of OCP, OCP/0.5 μg SDF-1, OCP/1.0 μg SDF-1, and OCP/5.0 μg SDF-1. The arrowheads indicate the edge of the defect. Arrows indicate osteocalcin-positive cells, and the asterisks indicate residual OCP granules. The open squares in the lower magnified images indicate the areas in the higher magnified images. The scale of the lower and higher magnified images is 2.5 mm and 100 μm, respectively. Quantitative analysis of the number of osteocalcin-positive cells in the ROI of the defect region (**Q**). (**$p < 0.01$, ***$p < 0.001$)

suggested that the structural features of OCP are related to the capacity of SDF-1 to be maintained on its surface. It has been confirmed that OCP tends to undergo a phase transformation to HA under physiological conditions [1, 2, 7] and that HA formed via this transformation is a non-stoichiometric CDHA with a lower Ca/P molar ratio (~1.5) [14] compared with that of stoichiometric HA (1.67). CDHA, prepared through original OCP hydrolysis, has a plate-like crystal morphology, similar to that of the original OCP [2, 14, 28, 65, 66], but different Ca/P ratios, SSA, and phases in the crystal, and is considered an appropriate control material for OCP [2, 66].

SDF-1 is produced by stromal cells in many tissues, including the bone, and is involved in many functions, including tissue development, angiogenesis, immune response, bone repair, neuronal regeneration, and many pathological conditions, including tumor cell migration and metastasis [67, 68]. SDF-1 interacts with CXCR4 receptors; in particular, CXCR4 receptor-positive MSCs have been reported to be strongly induced by SDF-1 in a dose-dependent manner [69]. SDF-1 increases the local blood supply by stimulating peripheral angiogenesis [70] and promotes osteogenic differentiation by upregulating BMP expression and directing MSCs to sites of injury and inflammation [71, 72]. SDF-1 promotes osteoclastogenesis [73, 74]. However, the biological effects of SDF-1 in combination with OCP bone substitute materials have never been studied.

The radiographic evaluation using micro-CT revealed that 2 weeks after implantation, the OCP/1.0 µg SDF-1 group exhibited better new bone formation compared with the OCP-only and the OCP/0.5 µg SDF-1 groups. At 2 weeks, the BMD in the OCP/SDF-1 1.0 µg group was significantly higher compared to the other groups, except for the OCP/SDF-1 0.5 µg group. In contrast, at 4 weeks post-implantation, there were no significant differences among the groups, indicating successful bone formation (Figs. 4 and 5). The ability of SDF-1-loaded OCP to enhance bone formation may be attributed to its ability to induce MSCs to migrate to the bone defect site early after implantation and to promote the differentiation and activation of osteoblasts. However, at 4 weeks after implantation, all groups showed good bone formation with no significant differences, likely due to the inherent properties of OCP, which induce MSCs to promote their differentiation into osteoblasts, and activate them effectively.

At the 2 weeks after implantation, the OCP/1.0 µg SDF-1 group showed a significant decrease in the remaining amount of OCP compared with the OCP-only and the OCP/0.5 µg SDF-1 groups, indicating enhanced biodegradability. Furthermore, the improvement in biodegradability due to SDF-1 was still evident at the 4 weeks after implantation (Figs. 4 and 5). These results suggest that SDF-1 collaboratively induces MSCs to migrate to the bone defect site, enhances their differentiation and activation into osteoblasts, and promotes the degradation of OCP within the rat femur. This is consistent with the previously reported characteristics of the degradation process of OCP, differentiating and activating osteoblasts [40, 45]. The tendency that the new bone volume was decreased in 4 weeks as compared to 2 weeks could be explained by the bone remodeling in the intramedullary canal of the tibia: (1) the new bone formed around OCP is resorbed accompanied by OCP degradation and (2) the new bone formed reactively due to the defect creation in tibia tends to be resorbed as observed in OCP or HA implantations in rabbit bone marrow [75].

Histological examinations confirmed similar trends to the micro-CT analysis. In histological examinations, at the 2 weeks after implantation, the OCP/1.0 µg SDF-1 group exhibited superior bone formation ability and biodegradability compared with the OCP-only, OCP/0.5 µg SDF-1, and even the OCP/5.0 µg SDF-1 groups (Figs. 6–8). Osteocalcin immunostaining demonstrated a significant increase in osteocalcin-positive cells in the OCP/SDF-1 1.0 µg group at 2 weeks compared to the OCP-alone group and other OCP/SDF-1 conditions. This finding supports the validity of the histological assessment indicating the bone formation-promoting effect of the OCP/SDF-1 1.0 µg group (Fig. 11). Regarding the biodegradability of SDF-1-loaded OCPs, the OCP/1.0 µg SDF-1 group, in particular, showed a benefit in osteoclast-like cell differentiation and activation compared with the OCP alone group and other doses of SDF-1-loaded OCP groups. This is supported by the fact that the expression of CXCR4, a receptor for SDF-1, is dependent on the concentration of SDF-1. Since OCP/1.0 µg SDF-1 promotes CXCR4 expression the most, it is assumed to effectively promote new bone formation and OCP degradation. SDF-1 has been shown to enhance the differentiation of osteoblasts and osteoclasts [76, 77], indicating the possibility of a unique mechanism that synergistically boosts osteoblast differentiation and osteoclastogenic capabilities of OCPs [34, 37]. These results suggest that SDF-1 not only enhances the bone formation ability and biodegradability of OCP in a dose-dependent manner but that there might be an optimal concentration for its effectiveness. SDF-1 is known to have a concentration-dependent effect in attracting endogenous MSCs to the injury site, thereby contributing to on-site tissue repair [78]. However, it has also been reported that implantation of SDF-1-loaded bone graft substitutes into bone defects induces osteogenesis at optimal concentrations but inhibits osteogenesis at higher concentrations [79]. This study suggested that OCP at 5.0 mg when loaded with 1.0 µg SDF-1, has superior MSC migration ability compared with larger volumes of SDF-1 loading. The OCP/1.0 µg SDF-1

group demonstrated superior bone formation and biodegradability compared with the other groups. Previous studies have reported excellent bone formation with samples modified using a 1.0 µg/mL SDF-1 solution [79, 80]. As mentioned above, it has been recognized that SDF-1 has an optimal concentration for osteoblast differentiation [79]. OCP increases RANKL expression in osteoblasts and forms osteoclasts on its surface from co-culture of bone marrow-derived cells and osteoblasts [37]. Although it is still unclear how SDF-1 dose affects the cellular function of accumulated MSCs around OCPs regarding osteoclastogenesis, higher concentrations of SDF-1 may have influenced the resorption of OCP itself through osteoclast formation, as shown in Fig. 8B (r-Implant %) and Fig. 9Q (TRAP-positive cell number), thereby controlling new bone formation. This is a topic for future consideration.

The present study investigated the effect of SDF-1 released from OCP on a mouse bone marrow-derived MSC line in vitro. In the migration assay, OCP loading 1.0 µg SDF-1 enhanced migration of the MSC compared with 1.0 µg SDF-1 dissolved in the media without OCP (Fig. 2A). The concentration of SDF-1 released from OCP increased during the incubation period from 0 to 24 h. The SDF-1 concentration gradient is the driving force for MSC migration [81–83]. An environment with a uniform concentration of SDF-1 suppressed MSC migration in a Transwell assay [81]. Thus, the released SDF-1 may induce a gradient of SDF-1 concentration from the OCP, resulting in enhanced MSC migration to OCP by the SDF-1 loading. Furthermore, the mechanism by which the SDF-1 loading amount onto OCP regulates MSC migration was examined. The migration rate increased from 0 to 1.0 µg SDF-1 loaded onto the OCP (Fig. 2A). However, OCP/5.0 µg SDF-1, which rapidly increased SDF-1 concentration in the media, inhibited cell migration (Fig. 2B, C). Previous studies have reported that increasing SDF-1 concentration promotes MSC migration in the range of 0–150 ng/mL SDF-1 [84, 85]. Although the response of migration to SDF-1 concentration depends on the cell type, desensitization to SDF-1 is induced by overstimulation at higher concentrations [86–88]. In the cell migration response to SDF-1 released from polymer nanoparticles, suppression of SDF-1 burst release increases neural progenitor/stem cell migration [87]. Based on these previous studies, the migration assay and SDF-1 release tests suggest that OCP/1.0 µg SDF-1 may show suitable sustained release of SDF-1 for the stimulation of MSC migration to the OCP granules.

Protein loading by lyophilization allows the protein to be easily released from calcium phosphate [89]. However, burst release from OCP/0.5 and 1.0 µg SDF-1 was not observed. OCP adsorbs a basic protein, such as cytochrome c and lysozyme, in physiological conditions [90, 91]. Part of the SDF-1 interacted with the surface during the loading process of SDF-1 using lyophilization. The released SDF-1 was also partially adsorbed onto OCP in the culture medium. In the FTIR spectra, the amount of protein absorbed from the culture medium was detected in OCP/SDF-1 at 48 h (Fig. 3). In contrast, OCP gradually changes to an apatite structure in cell culture and in vivo [1, 2, 27, 29]. A previous report showed that the capacity and affinity of OCP for serum proteins were higher than CDHA [14]. Therefore, we examined whether the adsorption affinity and capacity of OCP for SDF-1 during the hydrolysis reaction were involved in the release of SDF-1 from OCP compared with CDHA.

The SDF-1 isotherms of OCP and CDHA were analyzed in the buffer at the initial concentration of SDF-1 in the range from 0.05 to 0.5 µg/mL based on the released SDF-1 concentration from OCP/1.0 µg SDF-1 and CDHA/1.0 µg SDF-1 (Fig. 2B, C). The SDF-1 adsorption isotherms of OCP and CDHA were well approximated by the Freundlich equation, but they did not fit the Langmuir equation in the present study (Fig. 2E). In these SDF-1 isotherms, the saturation of adsorption was not observed. However, the bovine serum albumin adsorption isotherms for OCP and CDHA were well explained by the Langmuir equation with adsorption saturation [14]. If SDF-1 adsorption becomes saturated on OCP and CDHA at higher equilibrium concentrations, the present SDF-1 adsorption could be in a lower equilibrium concentration range. It is possible that the measurements in the lower concentration region included some errors in the Langmuir plot, resulting in a decrease in the correlation coefficient in the approximation. It has been shown that Freundlich's isotherm equation is successfully used to approximate the isotherm around the lower and middle range of equilibrium concentration [92, 93]. The isotherms, approximated using Freundlich's equation, indicated that the adsorption capacity of OCP for SDF-1 was higher than that of CDHA for SDF-1 (Fig. 2E, Table 1). The value of K_f in the equation indicates the adsorption capacity [94].

In cell culture media, CDHA promoted the release of SDF-1 compared with OCP for 3–6 h, the same amount of SDF-1 was loaded onto these granules (Fig. 2D). These results suggest that the lower release rate of SDF-1 from OCP at the initial stage of incubation is due to the higher adsorption capacity of OCP, which has an intrinsic surface capacity for SDF-1. In the FTIR spectra, a decrease in the infrared absorption intensity attributed to HPO_4 [95] (Fig. 3) indicates that the hydrolysis of OCP partially progressed for 48 h. The DS values in the media incubated with OCP and OCP/SDF-1 (Table 2) with respect to OCP and HA also indicated that the culture media could potentially induce the transformation from OCP to the HA phase [29]. The decreasing tendency of adsorption capacity with the progressive conversion from OCP to CDHA could increase the

release of SDF-1 adsorbed during the incubation in the culture medium. OCP/1.0 μg SDF-1 promoted the MSCs migration compared with CDHA/1.0 μg SDF-1 in the in vitro cell assay (Fig. 2A). Therefore, SDF-1 release, controlled by the progressive structural conversion of OCP to CDHA, could be the mechanism leading to the enhancement of MSC migration and subsequent bone regeneration around the OCP in rat femur defects.

The present in vitro study did not show a substantial conversion of OCP (Table 2, Fig. 3) because of a possible inhibition mechanism by SDF-1 adsorption. Although the present in vivo study did not investigate the conversion tendency of the implanted materials, because OCP has been shown to convert to the apatite phase in vitro and in vivo in previous studies [1, 2, 27, 29], it is reasonable to assume that the phase conversion of OCP in OCP/SDF-1 implantation takes place in an in vivo environment where Ca^{2+} and Pi ions are constantly supplied, and where a small amount of F^- ions, which promote the hydrolysis of OCP [7, 14, 96, 97], are also included. OCP is resorbed by osteoclast-like cells in vivo [75]. Therefore, the release of SDF-1 from OCP, associated with the cellular biodegradation of OCP, can also be expected to enhance bone regeneration through the synergetic effect of OCP and SDF-1.

5 Conclusion

In this study, we used SDF-1 to clarify the synergistic effect of its combination with OCP on MSC migration toward OCP-implanted bone regeneration. The intrinsic cellular activation properties of OCP were augmented by the possible adsorption of SDF-1 onto the OCP surface. These effects were confirmed to be the highest at specific SDF-1 doses, which are commonly observed in MSC migration, bone formation, and material biodegradation. It has been suggested that the structure and surface molecular affinity of OCP are related to the retention and sustained release of SDF-1. The synergistic effects of OCP and SDF-1 are expected to positively affect bone regeneration in various bone defects, including large bone defects, in many clinical situations.

Data availability

The raw/processed data required to reproduce these findings cannot be shared at this time, as the data also form part of an ongoing study.

Acknowledgements This work was supported in part by MEXT/JSPS KAKENHI Grant Numbers JP21K19586, JP21H03121, and JP24K02624. The authors thank Japan Fine Ceramics Co. Ltd. (JFC)/JGC Holdings Corp. (JHD) for the Joint Research Project in relation to this study.

Author contributions Ryuichi Kanabuchi: Investigation, validation, writing – original draft, formal analysis, and visualization. Ryo Hamai: Methodology, validation, data curation, writing – original draft, and writing – review & editing. Yu Mori: Methodology, validation, writing – original draft, and writing – review & editing. Soshi Hamada: Investigation, formal analysis, and visualization. Yukari Shiwaku: Validation, writing – review & editing. Yuko Sai: Validation, writing – review & editing. Kaori Tsuchiya: Validation, data curation, and writing – review & editing. Toshimi Aizawa: Writing – review & editing. Osamu Suzuki: Conceptualization, methodology, validation, data curation, writing – original draft, with – review & editing, supervision, project administration, and funding acquisition.

Compliance with ethical standards

Conflict of interest The authors declare no competing interests.

Ethical approval Research involving Human Participants and/or Animals: This research includes animal studies. All animal experiments were approved by the Animal Research Committee of Tohoku University (Approval No. 2021DnA-029-01) and conducted in accordance with institutional guidelines. The study adhered to the ARRIVE guidelines.

Informed consent This research does not include the study involving human participation.

Publisher's note Springer Nature remains neutral with regard to jurisdictional claims in published maps and institutional affiliations.

References

1. Suzuki O, Nakamura M, Miyasaka Y, Kagayama M, Sakurai M. Bone formation on synthetic precursors of hydroxyapatite. Tohoku J Exp Med. 1991;164:37–50. https://doi.org/10.1620/tjem.164.37
2. Suzuki O, Kamakura S, Katagiri T, Nakamura M, Zhao B, Honda Y, et al. Bone formation enhanced by implanted octacalcium phosphate involving conversion into Ca-deficient hydroxyapatite. Biomaterials. 2006;27:2671–81. https://doi.org/10.1016/j.biomaterials.2005.12.004
3. Kawai T, Kamakura S, Matsui K, Fukuda M, Takano H, Iino M, et al. Clinical study of octacalcium phosphate and collagen composite in oral and maxillofacial surgery. J Tissue Eng. 2020;11:2041731419896449. https://doi.org/10.1177/2041731419896449

4. Komlev VS, Popov VK, Mironov AV, Fedotov AY, Teterina AY, Smirnov IV, et al. 3D printing of octacalcium phosphate bone substitutes. Front Bioeng Biotechnol. 2015;3:81. https://doi.org/10.3389/fbioe.2015.00081
5. Kovrlija I, Locs J, Loca D. Octacalcium phosphate: Innovative vehicle for the local biologically active substance delivery in bone regeneration. Acta Biomater. 2021;135:27–47. https://doi.org/10.1016/j.actbio.2021.08.021
6. Brown WE, Smith JP, Lehr JR, Frazier AW. Octacalcium phosphate and hydroxyapatite: crystallographic and chemical relations between octacalcium phosphate and hydroxyapatite. Nature. 1962;196:1050–5. https://doi.org/10.1038/1961050a0
7. Brown W, Mathew M, Tung M. Crystal chemistry of octacalcium phosphate. Prog Cryst Growth Charact. 1981;4:59–87. https://doi.org/10.1016/0146-3535(81)90048-4
8. Brown WE. Crystal growth of bone mineral. Clin Orthop Relat Res. 1966;44:205–20.
9. Simon P, Grüner D, Worch H, Pompe W, Lichte H, El Khassawna T, et al. First evidence of octacalcium phosphate@osteocalcin nanocomplex as skeletal bone component directing collagen triple-helix nanofibril mineralization. Sci Rep. 2018;8:13696. https://doi.org/10.1038/s41598-018-31983-5
10. Miyatake N, Kishimoto KN, Anada T, Imaizumi H, Itoi E, Suzuki O. Effect of partial hydrolysis of octacalcium phosphate on its osteoconductive characteristics. Biomaterials. 2009;30:1005–14. https://doi.org/10.1016/j.biomaterials.2008.10.058
11. Addadi L, Weiner S. Control and design principles in biological mineralization. Angew Chem Int Ed Engl. 1992;31:153–69. https://doi.org/10.1002/anie.199201531
12. Suzuki O, Nakamura M, Miyasaka Y, Kagayama M, Sakurai M. Maclura pomifera agglutinin-binding glycoconjugates on converted apatite from synthetic octacalcium phosphate implanted into subperiosteal region of mouse calvaria. Bone Miner. 1993;20:151–66. https://doi.org/10.1016/s0169-6009(08)80024-4
13. Füredi-Milhofer H, Moradian-Oldak J, Weiner S, Veis A, Mintz KP, Addadi L. Interactions of matrix proteins from mineralized tissues with octacalcium phosphate. Connect Tissue Res. 1994;30:251–64. https://doi.org/10.3109/03008209409015041
14. Suzuki O, Yagishita H, Yamazaki M, Aoba T. Adsorption of bovine serum albumin onto octacalcium phosphate and its hydrolyzates. Cells Mater. 1995;5:45–54.
15. Combes C, Rey C, Freche M. In vitro crystallization of octacalcium phosphate on type I collagen: influence of serum albumin. J Mater Sci Mater Med. 1999;10:153–60. https://doi.org/10.1023/A:1008933406806
16. Kaneko H, Kamiie J, Kawakami H, Anada T, Honda Y, Shiraishi N, et al. Proteome analysis of rat serum proteins adsorbed onto synthetic octacalcium phosphate crystals. Anal Biochem. 2011;418:276–85. https://doi.org/10.1016/j.ab.2011.07.022
17. Akiva A, Malkinson G, Masic A, Kerschnitzki M, Bennet M, Fratzl P, et al. On the pathway of mineral deposition in larval zebrafish caudal fin bone. Bone. 2015;75:192–200. https://doi.org/10.1016/j.bone.2015.02.020
18. Akiva A, Kerschnitzki M, Pinkas I, Wagermaier W, Yaniv K, Fratzl P, et al. Mineral formation in the larval zebrafish tail bone occurs via an acidic disordered calcium phosphate phase. J Am Chem Soc. 2016;138:14481–7. https://doi.org/10.1021/jacs.6b09442
19. Markovic M. Octacalcium phosphate carboxylates. Monogr Oral Sci. 2001;18:77–93. https://doi.org/10.1159/000061649
20. Monma H, Goto M. Succinate-complexed octacalcium phosphate. Bull Chem Soc Jpn. 1983;56:3843–4. https://doi.org/10.1246/bcsj.56.3843
21. Yokoi T, Watanabe M, Nakamura F, Kimura-Suda H, Shimabukuro M, Kawashita M. Formation of octacalcium phosphate with incorporated dicarboxylate ions containing disulfide bonds. Dalton Trans. 2023;52:16586–90. https://doi.org/10.1039/d3dt02462h
22. Kovrlija I, Pańczyszyn E, Demir O, Laizane M, Corazzari M, Locs J, et al. Doxorubicin loaded octacalcium phosphate particles as controlled release drug delivery systems: Physico-chemical characterization, in vitro drug release and evaluation of cell death pathway. Int J Pharm. 2024;653:123932. https://doi.org/10.1016/j.ijpharm.2024.123932
23. Chaiariyakul D, Hamai R, Shiwaku Y, Tsuchiya K, Suzuki O. Adsorption behavior and osteoblastic cellular activity of metronidazole molecule with octacalcium phosphate and hydroxyapatite materials. J Drug Deliv Sci Technol. 2023:105046. https://doi.org/10.1016/j.jddst.2023.105046.
24. Eidelman N, Chow LC, Brown WE. Calcium phosphate phase transformations in serum. Calcif Tissue Int. 1987;41:18–26. https://doi.org/10.1007/bf02555126
25. Eidelman N, Chow LC, Brown WE. Calcium phosphate saturation levels in ultrafiltered serum. Calcif Tissue Int. 1987;40:71–78. https://doi.org/10.1007/BF02555708
26. Driessens F. Physiology of hard tissues in comparison with the solubility of synthetic calcium phosphates. Ann N. Y Acad Sci. 1988;523:131–6. https://doi.org/10.1111/j.1749-6632.1988.tb38507.x
27. Ban S, Jinde T, Hasegawa J. Phase transformation of octacalcium phosphate in vivo and in vitro. Dent Mater J. 1992;11:130–40. https://doi.org/10.4012/dmj.11.130
28. Suzuki O, Kamakura S, Katagiri T. Surface chemistry and biological responses to synthetic octacalcium phosphate. J Biomed Mater Res B Appl Biomater. 2006;77:201–12. https://doi.org/10.1002/jbm.b.30407
29. Sakai S, Anada T, Tsuchiya K, Yamazaki H, Margolis HC, Suzuki O. Comparative study on the resorbability and dissolution behavior of octacalcium phosphate, β-tricalcium phosphate, and hydroxyapatite under physiological conditions. Dent Mater J. 2016;35:216–24. https://doi.org/10.4012/dmj.2015-255
30. LeGeros RZ, Daculsi G, Orly I, Abergas T, Torres W. Solution-mediated transformation of octacalcium phosphate (OCP) to apatite. Scanning Microsc. 1989;3:129–37.
31. Suzuki O, Yagishita H, Amano T, Aoba T. Reversible structural changes of octacalcium phosphate and labile acid phosphate. J Dent Res. 1995;74:1764–9. https://doi.org/10.1177/00220345950740110801
32. Habraken WJ, Tao J, Brylka LJ, Friedrich H, Bertinetti L, Schenk AS, et al. Ion-association complexes unite classical and non-classical theories for the biomimetic nucleation of calcium phosphate. Nat Commun. 2013;4:1507. https://doi.org/10.1038/ncomms2490
33. Masuda T, Maruyama H, Arai F, Anada T, Tsuchiya K, Fukuda T, et al. Application of an indicator-immobilized-gel-sheet for measuring the pH surrounding a calcium phosphate-based biomaterial. J Biomater Appl. 2017;31:1296–304. https://doi.org/10.1177/0885328217699108
34. Anada T, Kumagai T, Honda Y, Masuda T, Kamijo R, Kamakura S, et al. Dose-dependent osteogenic effect of octacalcium phosphate on mouse bone marrow stromal cells. Tissue Eng Part A. 2008;14:965–78. https://doi.org/10.1089/tea.2007.0339
35. Sai Y, Shiwaku Y, Anada T, Tsuchiya K, Takahashi T, Suzuki O. Capacity of octacalcium phosphate to promote osteoblastic differentiation toward osteocytes in vitro. Acta Biomater. 2018;69:362–71. https://doi.org/10.1016/j.actbio.2018.01.026
36. Saito S, Hamai R, Shiwaku Y, Hasegawa T, Sakai S, Tsuchiya K, et al. Involvement of distant octacalcium phosphate scaffolds in enhancing early differentiation of osteocytes during bone regeneration. Acta Biomater. 2021;129:309–22. https://doi.org/10.1016/j.actbio.2021.05.017
37. Takami M, Mochizuki A, Yamada A, Tachi K, Zhao B, Miyamoto Y, et al. Osteoclast differentiation induced by synthetic

octacalcium phosphate through receptor activator of NF-kappaB ligand expression in osteoblasts. Tissue Eng Part A. 2009;15:3991–4000. https://doi.org/10.1089/ten.TEA.2009.0065
38. Hirayama B, Anada T, Shiwaku Y, Miyatake N, Tsuchiya K, Nakamura M, et al. Immune cell response and subsequent bone formation induced by implantation of octacalcium phosphate in a rat tibia defect. RSC Adv. 2016;6:57475–84. https://doi.org/10.1039/c6ra10834b
39. Kurobane T, Shiwaku Y, Anada T, Hamai R, Tsuchiya K, Baba K, et al. Angiogenesis involvement by octacalcium phosphate-gelatin composite-driven bone regeneration in rat calvaria critical-sized defect. Acta Biomater. 2019;88:514–26. https://doi.org/10.1016/j.actbio.2019.02.021
40. Okuyama K, Shiwaku Y, Hamai R, Mizoguchi T, Tsuchiya K, Takahashi T, et al. Differentiation of committed osteoblast progenitors by octacalcium phosphate compared to calcium-deficient hydroxyapatite in Lepr-cre/Tomato mouse tibia. Acta Biomater. 2022;142:332–44. https://doi.org/10.1016/j.actbio.2022.02.016
41. Giannoudis PV, Dinopoulos H, Tsiridis E Bone substitutes: an update. Injury. 2005;36 Suppl 3. https://doi.org/10.1016/j.injury.2005.07.029.
42. McAllister BS, Haghighat K. Bone augmentation techniques. J Periodontol. 2007;78:377–96. https://doi.org/10.1902/jop.2007.060048
43. Urist MR. Bone: formation by autoinduction. Science. 1965;150:893–9. https://doi.org/10.1126/science.150.3698.893
44. Ozaki H, Hamai R, Shiwaku Y, Sakai S, Tsuchiya K, Suzuki O. Mutual chemical effect of autograft and octacalcium phosphate implantation on enhancing intramembranous bone regeneration. Sci Technol Adv Mater. 2021;22:345–62. https://doi.org/10.1080/14686996.2021.1916378
45. Suzuki O, Shiwaku Y, Hamai R. Octacalcium phosphate bone substitute materials: Comparison between properties of biomaterials and other calcium phosphate materials. Dent Mater J. 2020;39:187–99. https://doi.org/10.4012/dmj.2020-001
46. Hamai R, Sakai S, Shiwaku Y, Anada T, Tsuchiya K, Ishimoto T, et al. Octacalcium phosphate crystals including a higher density dislocation improve its materials osteogenecity. Appl Mater Today. 2022;26:101279. https://doi.org/10.1016/j.apmt.2021.101279
47. Suzuki O, Hamai R, Sakai S. The material design of octacalcium phosphate bone substitute: increased dissolution and osteogenecity. Acta Biomater. 2023;158:1–11. https://doi.org/10.1016/j.actbio.2022.12.046
48. Kawai T, Anada T, Masuda T, Honda Y, Sakai Y, Kato Y, et al. The effect of synthetic octacalcium phosphate in a collagen scaffold on the osteogenicity of mesenchymal stem cells. Eur Cells Mater. 2011;22:124–36. https://doi.org/10.22203/ecm.v022a10
49. Yun YR, Won JE, Jeon E, Lee S, Kang W, Jo H, et al. Fibroblast growth factors: biology, function, and application for tissue regeneration. J Tissue Eng. 2010;2010:218142. https://doi.org/10.4061/2010/218142
50. Sallusto F, Baggiolini M. Chemokines and leukocyte traffic. Nat Immunol. 2008;9:949–52. https://doi.org/10.1038/ni.f.214
51. Melchers F, Rolink AG, Schaniel C. The role of chemokines in regulating cell migration during humoral immune responses. Cell. 1999;99:351–4. https://doi.org/10.1016/s0092-8674(00)81521-4
52. Murdoch C, Finn A. Chemokine receptors and their role in inflammation and infectious diseases. Blood. 2000;95:3032–43. https://doi.org/10.1182/blood.V95.10.3032
53. Zlotnik A, Yoshie O. Chemokines: a new classification system and their role in immunity. Immunity. 2000;12:121–7. https://doi.org/10.1016/s1074-7613(00)80165-x
54. Stich S, Haag M, Häupl T, Sezer O, Notter M, Kaps C, et al. Gene expression profiling of human mesenchymal stem cells chemotactically induced with CXCL12. Cell Tissue Res. 2009;336:225–36. https://doi.org/10.1007/s00441-009-0768-z
55. Thevenot PT, Nair AM, Shen J, Lotfi P, Ko CY, Tang L. The effect of incorporation of SDF-1alpha into PLGA scaffolds on stem cell recruitment and the inflammatory response. Biomaterials. 2010;31:3997–4008. https://doi.org/10.1016/j.biomaterials.2010.01.144
56. Zhang B, Li H, He L, Han Z, Zhou T, Zhi W, et al. Surface-decorated hydroxyapatite scaffold with on-demand delivery of dexamethasone and stromal cell derived factor-1 for enhanced osteogenesis. Mater Sci Eng C. 2018;89:355–70. https://doi.org/10.1016/j.msec.2018.04.008
57. Tsuchiya K, Hamai R, Sakai S, Suzuki O. Comparative analysis of bovine serum albumin adsorption onto octacalcium phosphate crystals prepared using different methods. Dent Mater J. 2020;39:883–91. https://doi.org/10.4012/dmj.2019-2250
58. Moreno EC, Kresak M, Zahradnik RT. Fluoridated hydroxyapatite solubility and caries formation. Nature. 1974;247:64–65. https://doi.org/10.1038/247064a0
59. Tung MS, Eidelman N, Sieck B, Brown WE. Octacalcium phosphate solubility product from 4 to 37 °C. J Res Natl Bur Stand. 1988;93:613–24. https://doi.org/10.6028/jres.093.153
60. Moreno EC, Brown WE, Osborn G. Solubility of dicalcium phosphate dihydrate in aqueous systems. Soil Sci Soc Am J. 1960;24:94–98. https://doi.org/10.2136/sssaj1960.03615995002400020009x
61. Moreno EC, Margolis HC. Composition of human plaque fluid. J Dent Res. 1988;67:1181–9. https://doi.org/10.1177/00220345880670090701
62. Aoba T, Moreno EC. The enamel fluid in the early secretory stage of porcine amelogenesis: chemical composition and saturation with respect to enamel mineral. Calcif Tissue Int. 1987;41:86–94. https://doi.org/10.1007/bf02555250
63. Hamada S, Mori Y, Shiwaku Y, Hamai R, Tsuchiya K, Baba K, et al. Octacalcium Phosphate/Gelatin Composite (OCP/Gel) enhances bone repair in a critical-sized transcortical femoral defect rat model. Clin Orthop Relat Res. 2022;480:2043–55. https://doi.org/10.1097/CORR.0000000000002257
64. Oizumi I, Hamai R, Shiwaku Y, Mori Y, Anada T, Baba K, et al. Impact of simultaneous hydrolysis of OCP and PLGA on bone induction of a PLGA-OCP composite scaffold in a rat femoral defect. Acta Biomater. 2021;124:358–73. https://doi.org/10.1016/j.actbio.2021.01.048
65. Chickerur NS, Tung MS, Brown WE. A mechanism for incorporation of carbonate into apatite. Calcif Tissue Int. 1980;32:55–62. https://doi.org/10.1007/BF02408521
66. Suzuki O. Octacalcium phosphate: osteoconductivity and crystal chemistry. Acta Biomater. 2010;6:3379–87. https://doi.org/10.1016/j.actbio.2010.04.002
67. Yang F, Xue F, Guan J, Zhang Z, Yin J, Kang Q. Stromal-cell-derived factor (SDF) 1-alpha overexpression promotes bone regeneration by osteogenesis and angiogenesis in osteonecrosis of the femoral head. Cell Physiol Biochem. 2018;46:2561–75. https://doi.org/10.1159/000489684
68. Elmansi AM, Eisa NH, Periyasamy-Thandavan S, Kondrikova G, Kondrikov D, Calkins MM, et al. DPP4-truncated CXCL12 alters CXCR4/ACKR3 signaling, osteogenic cell differentiation, migration, and senescence. ACS Pharmacol Transl Sci. 2023;6:22–39. https://doi.org/10.1021/acsptsci.2c00040
69. Sordi V, Malosio ML, Marchesi F, Mercalli A, Melzi R, Giordano T, et al. Bone marrow mesenchymal stem cells express a restricted set of functionally active chemokine receptors capable of promoting migration to pancreatic islets. Blood. 2005;106:419–27. https://doi.org/10.1182/blood-2004-09-3507
70. De Falco E, Porcelli D, Torella AR, Straino S, Iachininoto MG, Orlandi A, et al. SDF-1 involvement in endothelial phenotype and ischemia-induced recruitment of bone marrow progenitor cells.

Blood. 2004;104:3472–82. https://doi.org/10.1182/blood-2003-12-4423
71. Ma J, Ge J, Zhang S, Sun A, Shen J, Chen L, et al. Time course of myocardial stromal cell-derived factor 1 expression and beneficial effects of intravenously administered bone marrow stem cells in rats with experimental myocardial infarction. Basic Res Cardiol. 2005;100:217–23. https://doi.org/10.1007/s00395-005-0521-z
72. Miller RJ, Banisadr G, Bhattacharyya BJ. CXCR4 signaling in the regulation of stem cell migration and development. J Neuroimmunol. 2008;198:31–38. https://doi.org/10.1016/j.jneuroim.2008.04.008
73. Wright LM, Maloney W, Yu X, Kindle L, Collin-Osdoby P, Osdoby P. Stromal cell-derived factor-1 binding to its chemokine receptor CXCR4 on precursor cells promotes the chemotactic recruitment, development, and survival of human osteoclasts. Bone. 2005;36:840–53. https://doi.org/10.1016/j.bone.2005.01.021
74. Shima K, Kimura K, Ishida M, Kishikawa A, Ogawa S, Qi J, et al. C-X-C motif chemokine 12 enhances lipopolysaccharide-induced osteoclastogenesis and bone resorption in vivo. Calcif Tissue Int. 2018;103:431–42. https://doi.org/10.1007/s00223-018-0435-z
75. Imaizumi H, Sakurai M, Kashimoto O, Kikawa T, Suzuki O. Comparative study on osteoconductivity by synthetic octacalcium phosphate and sintered hydroxyapatite in rabbit bone marrow. Calcif Tissue Int. 2006;78:45–54. https://doi.org/10.1007/s00223-005-017
76. Zhu W, Liang G, Huang Z, Doty SB, Boskey AL. Conditional inactivation of the CXCR4 receptor in osteoprecursors reduces postnatal bone formation due to impaired osteoblast development. J Biol Chem. 2011;286:26794–805. https://doi.org/10.1074/jbc.M111.250985
77. Luo T, Liu H, Feng W, Liu D, Du J, Sun J, et al. Adipocytes enhance expression of osteoclast adhesion-related molecules through the CXCL12/CXCR4 signalling pathway. Cell Prolif. 2017;50:12317. https://doi.org/10.1111/cpr.12317
78. Marquez-Curtis LA, Janowska-Wieczorek A. Enhancing the migration ability of mesenchymal stromal cells by targeting the SDF-1/CXCR4 axis. Biomed Res Int. 2013;2013:561098. https://doi.org/10.1155/2013/561098
79. Seon JK, Kuppa SS, Kang JY, Lee JS, Park SA, Yoon TR, et al. Peptide derived from stromal cell-derived factor 1δ enhances the in vitro expression of osteogenic proteins via bone marrow stromal cell differentiation and promotes bone formation in in vivo models. Biomater Sci. 2023;11:6587–99. https://doi.org/10.1039/d3bm00798g
80. Lauer A, Wolf P, Mehler D, Gotz H, Ruzgar M, Baranowski A, et al. Biofabrication of SDF-1 functionalized 3D-printed cell-free scaffolds for bone tissue regeneration. Int J Mol Sci. 2020;21:2175. https://doi.org/10.3390/ijms21062175
81. Kitaori T, Ito H, Schwarz EM, Tsutsumi R, Yoshitomi H, Oishi S, et al. Stromal cell-derived factor 1/CXCR4 signaling is critical for the recruitment of mesenchymal stem cells to the fracture site during skeletal repair in a mouse model. Arthritis Rheumatol. 2009;60:813–23. https://doi.org/10.1002/art.24330
82. Won YW, Patel AN, Bull DA. Cell surface engineering to enhance mesenchymal stem cell migration toward an SDF-1 gradient. Biomaterials. 2014;35:5627–35. https://doi.org/10.1016/j.biomaterials.2014.03.070
83. Park S, Jang H, Kim BS, Hwang C, Jeong GS, Park Y. Directional migration of mesenchymal stem cells under an SDF-1α gradient on a microfluidic device. PLoS ONE. 2017;12:0184595. https://doi.org/10.1371/journal.pone.0184595
84. Gong J, Meng HB, Hua J, Song ZS, He ZG, Zhou B, et al. The SDF-1/CXCR4 axis regulates migration of transplanted bone marrow mesenchymal stem cells towards the pancreas in rats with acute pancreatitis. Mol Med Rep. 2014;9:1575–82. https://doi.org/10.3892/mmr.2014.2053
85. Ling L, Hou J, Liu D, Tang D, Zhang Y, Zeng Q, et al. Important role of the SDF-1/CXCR4 axis in the homing of systemically transplanted human amnion-derived mesenchymal stem cells (hAD-MSCs) to ovaries in rats with chemotherapy-induced premature ovarian insufficiency (POI). Stem Cell Res Ther. 2022;13:79. https://doi.org/10.1186/s13287-022-02759-6
86. Robin AM, Zhang ZG, Wang L, Zhang RL, Katakowski M, Zhang L, et al. Stromal cell-derived factor 1alpha mediates neural progenitor cell motility after focal cerebral ischemia. J Cereb Blood Flow Metab. 2006;26:125–34. https://doi.org/10.1038/sj.jcbfm.9600172
87. Dutta D, Fauer C, Mulleneux HL, Stabenfeldt SE. Tunable controlled release of bioactive SDF-1α via protein specific interactions within fibrin/nanoparticle composites. J Mater Chem B. 2015;3:7963–73. https://doi.org/10.1039/c5tb00935a
88. Signoret N, Oldridge J, Pelchen-Matthews A, Klasse PJ, Tran T, Brass LF, et al. Phorbol esters and SDF-1 induce rapid endocytosis and down modulation of the chemokine receptor CXCR4. J Cell Biol. 1997;139:651–64. https://doi.org/10.1083/jcb.139.3.651
89. Nandi SK, Kundu B, Mukherjee J, Mahato A, Datta S, Balla VK. Converted marine coral hydroxyapatite implants with growth factors: in vivo bone regeneration. Mater Sci Eng C. 2015;49:816–23. https://doi.org/10.1016/j.msec.2015.01.078
90. Shiwaku Y, Honda Y, Anada T, Morimoto S, Masuda T, Sasaki K, et al. Analysis of physicochemical properties of octacalcium phosphate prepared by hydrolysis and co-precipitation with fluoride ions. J Ceram Soc Jpn. 2010;118:402–5. https://doi.org/10.2109/jcersj2.118.402
91. Miyazaki T, Masuda K, Sakamoto K. Release profiles of dyes and proteins from calcium phosphate microspheres with different crystalline phases. Ceramics. 2021;4:291–301. https://doi.org/10.3390/ceramics4020023
92. Chen X. Modeling of experimental adsorption isotherm data. Information. 2015;6:14–22. https://doi.org/10.3390/info6010014
93. Vigdorowitsch M, Pchelintsev A, Tsygankova L, Tanygina E. Freundlich isotherm: an adsorption model complete framework. Appl Sci. 2021;11:8078. https://doi.org/10.3390/app11178078
94. Hashem A, Aniagor CO, Nasr MF, Abou-Okeil A. Efficacy of treated sodium alginate and activated carbon fibre for Pb(II) adsorption. Int J Biol Macromol. 2021;176:201–16. https://doi.org/10.1016/j.ijbiomac.2021.02.067
95. Fowler BO, Markovic M, Brown WE. Octacalcium phosphate. 3. Infrared and Raman vibrational spectra. Chem Mater. 1993;5:1417–23. https://doi.org/10.1021/cm00034a009
96. Tung MS, Tomazic B, Brown WE. The effects of magnesium and fluoride on the hydrolysis of octacalcium phosphate. Arch Oral Biol. 1992;37:585–93. https://doi.org/10.1016/0003-9969(92)90142-u
97. Mura-Galelli M, Narusawa H, Shimada T, Iijima M, Aoba T. Effects of fluoride on precipitation and hydrolysis of octacalcium phosphate in an experimental model simulating enamel mineralization during amelogenesis. Cells Mater. 1992;2:5